Phytoplankton assemblage structure and primary productivity along 170° W in the South Pacific Ocean

Giacomo R. DiTullio[1],*, Mark E. Geesey[1], David R. Jones[1,2], Kendra L. Daly[3], Lisa Campbell[4], Walker O. Smith Jr[5]

[1]**University of Charleston, Grice Marine Laboratory, Charleston, South Carolina 29412, USA**
[2]**Rutgers University, Haskins Shellfish Research Laboratory, Port Norris, New Jersey 08349, USA**
[3]**College of Marine Science, University of South Florida, St. Petersburg, Florida 33701, USA**
[4]**Department of Oceanography, Texas A&M University, College Station, Texas 77843-3146, USA**
[5]**Virginia Institute of Marine Science, College of William and Mary, Gloucester Point, Virginia 23602, USA**

ABSTRACT: Phytoplankton pigments were measured using HPLC during non-ENSO conditions in mid-summer along a South Pacific transect from 67° S to the equator along 170° W. Highest concentrations of chlorophyll *a* (chl *a*) occurred in the Polar and the Subtropical Fronts (PF and STF, respectively) with concentrations exceeding 500 ng l^{-1}. In the STF, there was a distinct subsurface chl *a* maximum (SCM) at 40 m, which gradually deepened northward to 120 m in the Subtropical Convergence Zone. Northwards, the SCM shoaled to about 30 m in the Equatorial Zone (EZ). Relatively high concentrations of fucoxanthin and 19′-butanoyloxyfucoxanthin occurred in the nutrient-rich waters south of the Subantarctic Front, and CHEMTAX analyses indicated that diatoms, chrysophytes, pelagophytes, and haptophytes dominated the phytoplankton assemblage. Northward of the PF to the STF, where silicate concentrations were <1 μM, pelagophytes and coccolithophorids dominated the water column; diatoms were virtually absent, and *Phaeocystis*, prasinophytes, cryptophytes, and chlorophytes contributed significantly to the total algal biomass. *Phaeocystis* populations were dominant at or below the 1% light level. In the South Pacific Gyre (SPG), *Synechococcus* (*Syn*) and *Prochlorococcus* (*Pro*) were major components of the phytoplankton assemblage with *Pro* dominant as indicated by both flow cytometry and by the ratio of divinyl chl *a*:total chl *a* (0.43 ± 0.07). Photoacclimation by *Pro* in the SPG was pronounced, with a higher average divinyl chl *a* per cell ratio in the SCM (1.1) relative to values (0.1) in the upper waters (0 to 100 m). Primary production rates exceeding 1 μg C l^{-1} h^{-1} occurred at the surface in the STF. Surface primary production rates were generally < 0.4 μg C l^{-1} h^{-1} across the SPG, but exceeded 1.4 μg C l^{-1} h^{-1} at the equator. In the EZ, *Pro* dominated the phytoplankton assemblage, but *Phaeocystis* and prasinophytes were also major constituents of the assemblage.

KEY WORDS: Phytoplankton assemblage · Photosynthetic pigments · Productivity · Antarctic Circumpolar Current · South Pacific Gyre · Equatorial upwelling · CHEMTAX

INTRODUCTION

Marine phytoplankton play a significant role in regulating global atmospheric CO_2 levels (Martin 1990, Cooper et al. 1996). At present, it is not clear how vital algal taxonomic composition is in controlling primary and new production in different oceanic regimes (Falkowski et al. 1998). Recent evidence, however, suggests that phytoplankton composition is intimately related to regional biogeochemical cycles (Falkowski

1994, Karl et al. 1997, Boyd & Newton 1999). For instance, differences in algal taxonomic composition can affect stoichiometric nutrient drawdown ratios in a particular region, such as in the Ross Sea (Arrigo et al. 1999, 2000), the California Upwelling region (Hutchins et al. 1999), and the Pacific sector of the Southern Ocean (Rubin et al. 1998). Similarly, zooplankton assemblage composition is a major determinant of elemental vertical flux to depth (Michaels & Silver 1988, Steinberg et al. 2000). Therefore, differences in the

phytoplankton composition may ultimately impact a region's response to seasonal or climatological changes (Karl 1999) and can lead to wide-scale changes in food web structure (Boyd & Newton 1999). Because of the importance of the South Pacific Ocean to estimates of global production and carbon budgets, determining phytoplankton taxonomic distributions and primary production rates are key to understanding various global biogeochemical processes. In the coming decades, global climate change processes may well cause a shift to occur in phytoplankton species composition in the Pacific Ocean (e.g. Karl 1999). Our ability to recognize the biogeochemical changes that will ensue following algal population shifts is dependent on our prior knowledge of the ecosystem.

As part of the NOAA-sponsored World Ocean Circulation Experiment (WOCE) and Joint Global Ocean Flux Study (JGOFS), we investigated phytoplankton composition in the South Pacific Ocean from 67° S to the Equator along 170° W. Along this transect existed a variety of oceanic ecosystems with wide variations in physical and chemical properties. During winter, deep-mixing events replenish these properties in the surface mixed layer, while in spring and summer the absolute quantities are governed by physical, chemical, and biological interactions including vertical turbulent diffusion of nutrients from deep water. In the Antarctic Circumpolar Current (ACC), summer mixed-layer depths are relatively shallower, nutrient concentrations are greater, and temperatures are considerably lower than in subtropical and tropical regions, and, not unexpectedly, the phytoplankton assemblage in the ACC is distinct from those further north (Furuya et al. 1986). For instance, eukaryotic phytoplankton dominate the cold waters of the Southern Ocean (Jacques 1989), whereas prokaryotic picoplankton species dominate the algal biomass in warm waters (DiTullio & Laws 1991, DiTullio et al. 1993, Campbell et al. 1994).

Latitudinal differences in temperature, nutrient availability, irradiance, grazing rates, and taxon-specific maximal growth rates are probably the most important parameters in determining the phytoplankton assemblage in a given locale. Diatoms and hapto-phytes, for example, with their generally higher nutrient requirements and relatively high maximal growth rates at low temperatures, tend to dominate in polar and subpolar regions (Kang & Fryxell 1991, Bidigare et al. 1996). In contrast, *Synechococcus* (*Syn*) and *Prochlorococcus* (*Pro*) spp. have adapted to growing in oligotrophic as well as Fe-limited, high-nutrient, low-chlorophyll (HNLC) tropical and subtropical regions (Olson et al. 1990, Campbell et al. 1994). Seasonal solar variations (Boyd et al. 1999) and vertical turbulent diffusion (Nelson & Smith 1991) dictate irradiance levels (Mitchell et al. 1991) and spectral quality (Glover 1985),

which govern algal community composition. Relaxation events after storms (i.e. reduced rates of vertical mixing) can lead to significant changes in algal community structure (DiTullio & Laws 1991). In subtropical waters, summer stratification can also lead to the development of large blooms of nitrogen-fixing *Trichodesmium* spp. (Karl et al. 1995). Thus, the main environmental factors determining algal species dominance vary spatially and temporally for different oceanographic regimes. In addition, the relative importance of co-limiting nutrients (DiTullio et al. 1993) and light limitation (Mitchell et al. 1991, Nelson & Smith 1991) on algal biomass and species composition can vary not only regionally but also seasonally (Boyd et al. 1999).

Several methods are available for determining the abundance and diversity of phytoplankton assemblages. While microscopic techniques allow for the identification of certain types of phytoplankton to the genus and species level, many flagellates will disintegrate during preservation (Gieskes & Kraay 1983) or will be too small and nondescript to identify. Epifluorescence microscopy can be useful to identify uniquely fluorescing cells such as *Syn*, but must be tailored to the individual group under study. Stoecker et al. (1994) reported that for the best enumeration of phytoplankton, no single fixation method is suitable for all taxa and a variety of fixatives are necessary for accurate estimates of cell numbers. In addition, microscopic cell counts are very labor-intensive and require a thorough knowledge of phytoplankton taxonomy. Flow cytometry can distinguish between some major groups of phytoplankton and bacteria, but is best used in conjunction with other techniques to get a more complete picture of the community composition. Recent advances in using genetic probes to identify the composition of a phytoplankton assemblage (Moon-van der Staay et al. 2000) show some promise in measuring the diversity of a community, but these methods are not simple to perform. In addition, it is also unlikely that the highly specific probes will recognize all the appropriate members of the community on which they are targeted and may underestimate their contribution to the total community.

Separating algal pigments via high-performance liquid chromatography (HPLC) and using specific diagnostic pigments as taxonomic markers within the phytoplankton assemblage is perhaps the easiest method for determining the relative importance of each taxonomic group. Previous studies have relied on the assumption that for a given pigment produced by a certain class of phytoplankton, all members of that class will contain the pigment in a constant, defined ratio to chlorophyll *a* (chl *a*) (Peeken 1997), despite the fact that these ratios may vary as a function of light,

nutrient status, or growth rate (e.g. Goericke & Montoya 1998). This approach precludes the importance of nutrient-limited or photoacclimation effects by a population of phytoplankton and assumes that all members of the class will contain the identical pigment ratio. Furthermore, by representing a class of phytoplankton using only 1 pigment or a limited number, the analysis excludes other class members that may not contain the specified pigment (Letelier et al. 1993).

The CHEMTAX (CHEMical TAXonomy) program (a matrix-factorization program for calculating algal abundances from concentrations of algal chemosystematic-marker photopigments) for the MATLAB™ matrix computing system advances our ability to quantify phytoplankton assemblage composition from HPLC-determined pigment concentrations and ratios (Mackey et al. 1996, Wright et al. 1996). It employs a wider suite of pigments and a greater number of phytoplankton classes than previously used. Although the investigator must input an initial pigment ratio for each taxonomic class, the program can alter the pigment ratios, within the bounds set by the investigator, to better match the relative pigment ratios found in the phytoplankton assemblage at a particular locale. This is especially valuable when variations in pigment ratios are expected, for instance, between surface and deeper phytoplankton communities where differences due to photoacclimation may exist, or along transects where latitudinal variations occur.

In 1996 we participated in a cruise on the South Pacific Ocean, extending from the Southern Ocean to the Equator, to assess the magnitude and spatial variability of chemical and biological distributions. Specifically, those processes that influenced carbon dynamics were investigated in detail, especially for the Southern Ocean (Daly et al. 2001). We hypothesized that broad spatial patterns of phytoplankton composition would be related to nutrient patterns over the same scales, and, in particular, we expected that the phytoplankton assemblage composition would reflect variations in iron and silicate distributions. Secondarily, limitations of other environmental constraints (such as macronutrients, irradiance, and vertical mixing) may also have affected primary productivity and the abundance of various phytoplankton taxa. We report here the large-scale distribution of phytoplankton composition and biomass, and the associated rates of biological production.

MATERIALS AND METHODS

The NOAA RV 'Discoverer' occupied stations at a nominal spacing of 30 nautical miles, south to north along the hydrographic section P15S (170° W) between January 15 and March 5, 1996 as part of WOCE (Fig. 1). Table 1 lists the abbreviations used throughout this manuscript. The transect originated in the AZ, crossed the 3 fronts of the ACC—the Southern Front (SF), the Polar Front (PF), and the Subantarctic Front (SAF)—entered the Subantarctic Zone (SAZ), crossed the Subtropical Front (STF), proceeded through the South Pacific Gyrel (SPG), and ended in the Equatorial Zone (EZ) (Fig. 1). CTD profiles were recorded at each station; bottle samples were collected for the measurement of salinity and temperature for CTD calibration.

Irradiance profiles were determined using spectroradiometer (MER 500, Biospherical Instruments) casts conducted each day at local noon. One CTD cast per day was conducted about 1 h before sunrise to collect seawater for the analysis of a suite of chemical and biological parameters. Sampling depths within the photic zone (100, 50, 30, 15, 5, 1, and 0.1% of surface irradiance) for this daily biological cast were estimated from the extinction coefficient measured the previous day. Trace-metal-clean techniques (i.e. Kevlar line, and 12 l Niskin bottles adapted for clean sampling with Teflon-coated springs and silicon rubber seals) were used to collect water samples for biological rate measurements

Table 1. Abbreviations used in this paper

Zones, fronts and features:	
ACC	Antarctic Circumpolar Current
AZ	Antarctic Zone
AZ(n)	Antarctic Zone north of the SF
AZ(s)	Antarctic Zone south of the SF
EZ	Equatorial Zone
HNLC	High-nutrient low-chlorophyll
PF	Polar Front
PFZ	Polar Frontal Zone
SAF	Subantarctic Front
SAZ	Subantarctic Zone
SCM	Subsurface chlorophyll maximum
SF	Southern Front
SPG	South Pacific Gyre
STF	Subtropical Front
Phytoplankton pigments:	
19but	19'-butanoyloxyfucoxanthin
19hex	19'-hexanoyloxyfucoxanthin
Allox	alloxanthin
Chl	chlorophyll
Chl-ide	chlorophyllide
DD	diadinoxanthin
DT	diatoxanthin
DV	divinyl
Fucox	fucoxanthin
Perid	peridinin
Ph-ide	phaeophorbide
Ph-tin	phaeophytin
Prasinox	prasinoxanthin
Viol	violaxanthin
Zeax	zeaxanthin

(Fitzwater et al. 1982). Properties measured from the biological casts included nutrients, cell counts via flow cytometry, primary production (^{13}C uptake), and phytoplankton pigment concentrations using HPLC.
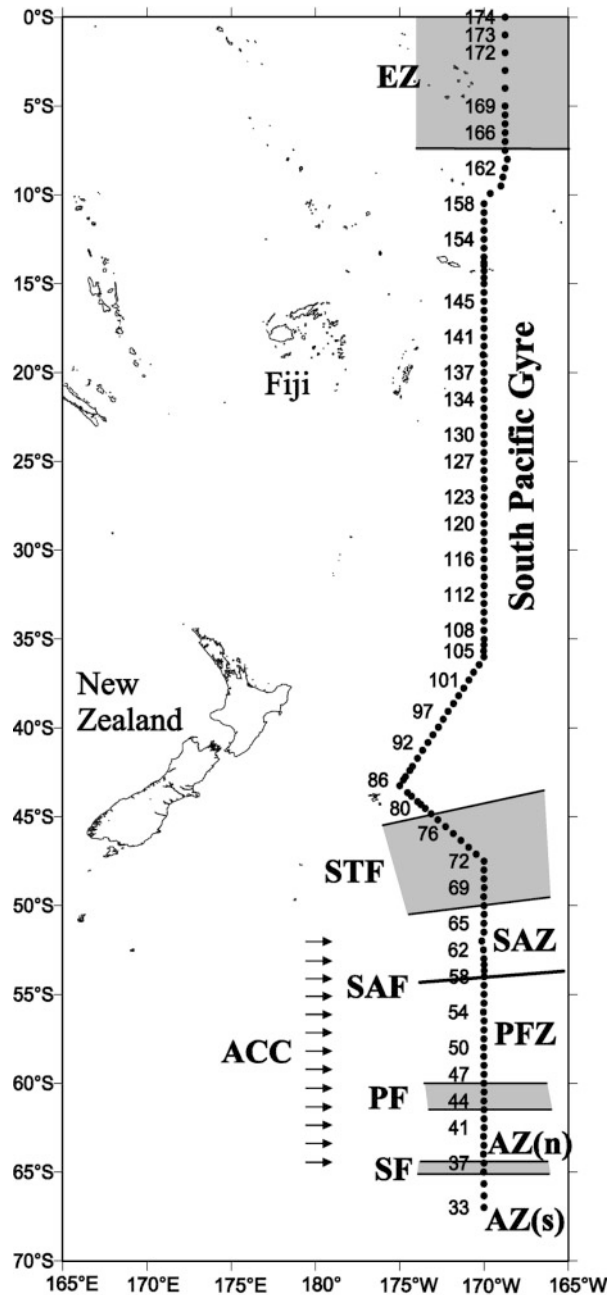

Fig. 1. WOCE (World Ocean Circulation Experiment) Transect P15S stations. Numbered stations are those from which biological samples were collected. Frontal positions after Daly et al. (2001): ACC (Antarctic Circumpolar Current), AZ(n) and AZ(s) (north and south Antarctic Zone), SF (Southern Front), PF (Polar Front), PFZ (Polar Frontal Zone, SAF (Subantarctic Front), SAZ (Subantarctic Zone), STF (Subtropical Front), EZ (Equatorial Zone)

Nutrient samples were analyzed for dissolved phosphate, silicic acid, nitrate, and nitrite using protocols of Gordon et al. (1993). Samples were measured using a modified Alpkem RFA 300 autoanalyzer. Analytical precision was determined from replicate analyses on 1 or more samples at almost every station. Urea measurements were made using an adaptation of the colorimetric method described in Mulvenna & Savidge (1992) using the diacetylmonoxime reaction. Ammonium measurements were made following the procedures outlined in Parsons et al. (1984).

Samples collected for flow cytometry were fixed with paraformaldehyde and kept frozen in liquid nitrogen until onshore processing (Campbell & Vaulot 1993). Cell numbers were enumerated following the procedure described in Campbell et al. (1994) using a FACSCalibur flow cytometer (Becton Dickinson), a dual-beam system (200 mW UV and 1 W 488 nm), to identify and count *Pro*, heterotrophic bacteria, *Syn*, and picoeukaryotic algae.

Primary production was measured using the ^{13}C incorporation method (Legendre & Gosselin 1996). Samples were collected in 1 l acid cleaned polycarbonate bottles, to which ca. 240 μmol H^{13}CO$_3$ (99% carrier-free; ICN) was added (approximately a 10% addition). All bottles were incubated on deck in incubators cooled with surface seawater to maintain constant temperature. Neutral-density screening was used to simulate light levels for bottle incubations. In addition, blue filters were used to spectrally simulate light levels below 30% surface irradiance (Laws et al. 1990). Incubation times for all productivity experiments were approximately from sunrise to sunset (ca. 12 to 17 h). After incubation, samples were filtered through GF/F filters, rinsed with a small volume of 0.01N HCl in seawater, and dried at 60°C. In the laboratory, samples were oxidized under vacuum to CO$_2$, and the resultant isotopic ratio was measured on a VG Isogas SIRA Series II mass spectrometer. All isotopic enrichments were converted to absolute units using the formulas of Legendre & Gosselin (1996). The average chl *a* concentration (initial and final time points from the incubation) was used in the calculation of the productivity index.

Photosynthetic pigments were separated on an automated Hewlett Packard 1050 HPLC with a MOS Hypersil reverse phase C-8 column using a ternary gradient with ammonium acetate as the ion pairing reagent (Wright et al. 1991, DiTullio & Geesey 2002). A diode array detector recorded pigment spectra every 5 s over the wavelengths 350 to 600 nm, and was set to record continuous chromatograms at 405 and 440 nm. An HP 1046A fluorescence detector with excitation of 421 nm and emission at 666 nm (optimized for chl *a*) was also employed to identify and quantify chl *a* and *c*,

as well as chl degradation products such as chl-ide, ph-ides, and ph-tin (see Table 1 for list of pigment abbreviations). The system was calibrated by repeated injections of pigment standards that were isolated from a variety of unialgal cultures maintained in the laboratory. Our method could not separate chl *b* and DV chl *b*, so unless otherwise noted the values reported here are for total chl *b* (i.e. the sum of these 2 forms).

Calculation of the relative abundance of various phytoplankton groups from the pigment concentrations was carried out using the CHEMTAX program (Mackey et al. 1996) written for the MATLAB™ matrix computing system. To account for photoacclimation and changes in pigment ratios with depth, samples were divided into depth bins for independent analysis by CHEMTAX. The depth bins used were: 0–10, 10–20, 20–30, 30–50, 50–75, 75–100, and 100–150 m. Samples falling into 2 bins (e.g. a 10 m sample) were included in both bins and the results were averaged. To account for geographical differences in the phytoplankton assemblage, samples were also divided into 2 latitudinal sections. A transition zone between the 2 sections was identified from 44 to 38° S (Stns 86 to 97) across which the depth of the 1% isolume increased from 60 to 100 m. South of the transition zone surface DV chl *a* concentration was 0, increasing to 30 ng l^{-1} within the transition zone and decreasing slightly further north. Surface concentrations of chl *a* and 19hex decreased precipitously across this zone, dropping from 200 to less than 25 ng l^{-1}. Other pigments had concentration decreases of the same magnitude. Samples collected from this zone were analyzed in both latitudinal sections and the results were averaged.

An initial pigment ratio matrix for each latitudinal section was created for incorporation into CHEMTAX (Table 2). While the best way to establish the pigment ratios for an algal class is to find a near-unialgal sample within the dataset, samples such as these are exceedingly rare; so the initial ratio matrix must be developed from reports of other analyses in the same environmental regime or from phytoplankton species cultured from the region under study. Our initial pigment ratio matrices were modified from the matrices reported in previous studies (Mackey et al. 1996, 1998, Higgins & Mackey 2000) with the addition of more algal classes (e.g. *Pro* and pelagophytes) and more pigments. Pigment ratios were modified based on published reports from field and culture studies, and from analyses of algal cultures maintained in various laboratories (see below).

The algal class Chrysophyceae has undergone considerable taxonomic revision over the last decade. Previous reports of the pigment compositions of chrysophytes (Jeffrey et al. 1997, Mackey et al. 1998) have included taxa such as *Synura* and *Pelagococcus* species, which have now been removed from this class. We developed our pigment ratios from data reported by Withers et al. (1981) and our own culture of *Ochromonas* spp. Most significantly, chrysophytes differ from pelagophytes and haptophytes by the absence of 19but. Pigment ratios for pelagophytes varied between the latitudinal sections. For the southern section we used ratios given by Wright & Jeffrey (1987) for an East Australian strain of *Pelagococcus subviridis* with equal amounts of 19but and Fucox as its primary carotenoids. For the northern section we derived our ratios from a North Pacific strain reported by Vesk & Jeffrey (1987) and a Sargasso Sea strain (CCMP1395) cultured in our laboratory. Jeffrey & Wright (1994) defined 4 types of haptopytes. Type 3 haptophytes (Hapto3) include coccolithophorids (e.g. *Emiliania huxleyii*) containing Fucox, large amounts of 19hex, and only trace amounts of 19but, while Type 4 haptophytes (Hapto4) represent taxa such as *Phaeocystis antarctica* that contain more equal ratios of Fucox, 19hex, and 19but. Pigment ratios for temperate/tropical versus polar strains were developed from a wide variety of sources (Wright & Jeffrey 1987, Jeffrey & Wright 1994, Stolte et al. 2000, S. W. Wright pers. comm.). Additional information regarding pigment ratios for prasinophytes came from Foss et al. (1986), Hooks et al. (1988), and our own culture of *Pycnococcus provasolii* (CCMP1198). Pigment ratios for *Pro* and *Syn* in the northern section were derived from the analysis of surface samples collected in the SPG where concentrations of pigments from eukaryotic algae (e.g. 19hex) were minimal.

In the mathematical analysis by CHEMTAX we allowed the pigment ratios to vary up to a maximum limit of 500% (i.e. 1/6 to 6 times the initial value). Weighting of the pigment concentrations was set to bound relative error by pigment with a weight bound of 30. Other settings included the iteration limit (500), the epsilon (residual) limit (0.005), the initial step size (10), the step ratio (1.3), the cutoff step (1000), the number of elements varied simultaneously (5), and the number of subiterations (5). The CHEMTAX output was the fraction of chl *a* contained in each algal group. The final portion of total chl *a* in each group was calculated by multiplying this fraction by the ratio of chl *a* to chl *a* + DV chl *a*. The portion of total chl *a* contained in *Pro* was simply the ratio of DV chl *a* to chl *a* + DV chl *a*.

RESULTS

CTD and nutrient sections

Following the methodology and terminology of Orsi et al. (1995), we used the CTD hydrographic properties

Table 2. Initial CHEMTAX pigment ratios for each taxonomic group. All ratios normalized to chlorophyll a, except for *Prochlorococcus* spp., which are normalized to DV chl a. Pigment abbreviations as in Table 1. Hapto3 and Hapto4 are Type 3 and Type 4 haptophytes as defined by Jeffrey & Wright (1994)

Group	chl a	DV chl a	Chl b	Chl c_1+c_2	Chl c_3	Perid	19but	Fucox	Viol	Prasinox	19hex	DD+DT	Allox	Zeax	Lutein
Northern Section															
Diatoms	1	0	0	0.2	0	0	0	0.934	0	0	0	0.288	0	0	0
Dinoflagellates	1	0	0	0.32	0	0.6	0	0	0	0	0	0.2	0	0	0
Cryptophytes	1	0	0	0.12	0	0	0	0	0	0	0	0	0.17	0	0
Chrysophytes	1	0	0	0.08	0.035	0	0	0.2	0.003	0	0.007	0.4	0	0	0
Pelagophytes	1	0	0	0.2	0.33	0	1.1	0.1	0	0	0.1	0.96	0	0	0
Hapto3	1	0	0	0.22	0.237	0	0.01	0.35	0	0	1.0	0.185	0	0	0
Hapto4	1	0	0	0.18	0.3	0	0.25	0.3	0	0	0.7	0.135	0	0	0
Prasinophytes	1	0	0.95	0	0	0	0	0	0.1	0.25	0	0	0	0.025	0.005
Chlorophytes	1	0	0.2	0	0	0	0	0	0.106	0	0	0	0	0.07	0.71
Synechococcus spp.	1	0	0	0	0	0	0	0	0	0	0	0	0	1.0	0
Prochlorococcus spp.	0	1	0.2	0	0	0	0	0	0	0	0	0	0	1.0	0
Southern Section															
Diatoms	1	0	0	0.2	0	0	0	0.75	0	0	0	0.14	0	0	0
Dinoflagellates	1	0	0	0.32	0	0.6	0	0	0	0	0	0.2	0	0	0
Cryptophytes	1	0	0	0.12	0	0	0	0	0	0	0	0	0.23	0	0
Chrysophytes	1	0	0	0.08	0.035	0	0	0.4	0.003	0	0.007	0.4	0	0	0
Pelagophytes	1	0	0	0.089	0.15	0	0.51	0.51	0	0	0.11	0.6	0	0	0
Hapto3	1	0	0	0.22	0.237	0	0.01	0.24	0	0	1.0	0.185	0	0	0
Hapto4	1	0	0	0.18	0.3	0	0.25	0.3	0	0	0.7	0.135	0	0	0
Prasinophytes	1	0	0.95	0	0	0	0	0	0.1	0.25	0	0	0	0.025	0.005
Chlorophytes	1	0	0.4	0	0	0	0	0	0.106	0	0	0	0	0.07	0.71
Synechococcus spp.	1	0	0	0	0	0	0	0	0	0	0	0	0	0.4	0
Prochlorococcus spp.	0	1	1.0	0	0	0	0	0	0	0	0	0	0	0.32	0

Table 3. General distribution pattern of various physical, chemical and biological core parameters in regimes of South Pacific Ocean during January to March 1996. Values for core parameters represent values measured within mixed layer for each specific region (mean ± SD). Dominant algal groups were determined using CHEMTAX analysis of HPLC pigment data. Abbreviations as in Table 1

Zone	Latitude (°S)	Station #	T (°C)	Salinity (psu)	Total chl a (ng l^{-1})	NO$_3$ (µM)	PO$_4$ (µM)	SiO$_4$ (µM)	Dominant algae
AZ(s)	>65	33 to 35	−0.687 ± 0.510	33.876 ± 0.214	145 ± 44	27.71 ± 0.60	1.87 ± 0.05	66.76 ± 1.46	Chrysophytes, diatoms, cryptophytes
SF	65 to 64	36 to 37	0.219 ± 0.063	33.884 ± 0.001	604	No data	No data	No data	Chrysophytes, diatoms
AZ(n)	64 to 62	38 to 42	0.735 ± 0.376	33.762 ± 0.050	463 ± 125	24.04 ± 0.10	1.38 ± 0.05	5.62 ± 0.82	Diatoms, chrysophytes, pelagophytes
PF	62 to 59	43 to 47	3.014 ± 0.931	33.849 ± 0.069	435 ± 139	23.06 ± 0.82	1.51 ± 0.03	1.05 ± 0.15	Diatoms, pelagophytes
PFZ	59 to 54	48 to 57	5.6715 ± 0.857	34.034 ± 0.053	257 ± 143	21.00 ± 0.93	1.38 ± 0.02	2.33 ± 1.97	Diatoms, pelagophytes, Hapto3, Hapto4
SAF	54	58	7.1125 ± 0.268	34.137 ± 0.004	118 ± 32	19.84 ± 0.06	1.34 ± 0.00	3.22 ± 0.17	Pelagophytes, Hapto3
SAZ	54 to 50	59 to 66	10.028 ± 0.300	34.362 ± 0.057	171 ± 92	12.62 ± 0.36	0.89 ± 0.03	0.96 ± 0.06	Pelagophytes, Hapto3, prasinophytes
STF	50 to 45	67 to 78	13.838 ± 1.395	34.619 ± 0.140	321 ± 82	2.85 ± 2.66	0.27 ± 0.19	0.70 ± 0.32	Hapto4, Hapto3, pelagophytes, prasinophytes
SPG	45 to 8	79 to 162	24.222 ± 4.301	35.280 ± 0.398	64 ± 66	0.03 ± 0.04	0.05 ± 0.05	1.32 ± 0.32	Prochlorophytes, Synechococcus, Hapto4
EZ	8 to 0	163 to 174	27.755 ± 1.102	35.521 ± 0.151	145 ± 64	3.38 ± 1.68	0.41 ± 0.11	2.43 ± 0.55	Hapto4, Prochlorophytes

to identify the regions and oceanic fronts crossed along the transect (Daly et al. 2001). Temperature stratification occurred in the STF (45 to 40°S) at 30 to 50 m (Fig. 2A) and deepened northward into the SPG. The average temperature increased northward across the frontal zones and into the SPG; it reached a maximum in the SPG and decreased slightly in the EZ, presumably due to upwelling (Fig. 2A). Little vertical structure in salinity distributions occurred in the upper 150 m, except in the central part of the SPG (Fig. 2B). The average salinity increased northward across the fronts and into the southern part of the SPG (Table 3), decreased in the central axis region due to precipitation (Hansell & Feely 2000), but increased again upon entering the EZ (Fig. 2B).

Both nitrate and phosphate concentrations decreased northward across the fronts and into the SPG, dropping to below detectable levels (<0.1 µM) in the SPG (Fig. 3A,B, Table 3). Concentrations of both nutrients rose slightly in the EZ. Silicate concentrations were highest (>60 µM) at the southernmost (ca. 67°S) station (#33), and decreased markedly across the SF (Fig. 3C, Table 3). Low silicate concentrations (<1 µM) were measured north of the STF. Ammonium concentrations were greatest (ca. 1 µM) between 70 and 100 m in the SF, SAF, and STF (Fig. 3D). In the SPG, NH_4^+ levels were typically undetectable (<0.1 µM), but slightly greater concentrations were found in the EZ. Urea concentrations were typically at or below our detection limits (<0.1 µM) and did not reveal any significant relationships with depth or oceanographic province (data not shown).

Pigment concentrations

The SAF generally contained lower pigment concentrations than the zones and fronts to the north or south. Surface chl *a* concentrations in the SAF were only 27 and 36 % of the concentrations in the PF and STF (Table 3), and depth-integrated chl *a* was 30 and 42 %, respectively (Table 4). In the STF, at about the depth of the 1 % isolume (45 m), we observed a subsurface chlorophyll maximum (SCM), deepening northward to about 120 m between 20 and 10° S (Fig. 4A). The SCM dissipated near the Equator. Chl *a* concentrations exceeded 500 ng l^{-1} in the PF and STF, while elsewhere concentrations rarely exceeded 300 ng l^{-1}. In the southern part of the SPG, chl *a* concentrations in the SCM were much greater than in the central and northern parts, where concentrations never exceeded 200 ng l^{-1} and usually were less than 100 ng l^{-1}. In the SPG north of 32°S, the amount of chl *a* in the upper 100 m was about equal to the chl *a* biomass in the 100 to 150 m depth zone (Table 5). In the EZ, however, there was 3.5-fold more chl *a* biomass above 100 m than between 100 and 150 m.

Although our HPLC method could not quantitatively separate chl *b* from DV chl *b*, we could identify the spectra of both forms in nearly all samples from the SCM of the SPG. In contrast, only the spectrum of monovinyl chl *b* was observed in the STF region. Therefore, what is reported for the SPG is total chl *b* (i.e. the sum of chl *b* and DV chl *b*). Chl *b* concentrations were minimal (<100 ng l^{-1}) south of the SAZ (Fig. 4B). In the STF, chl *b* concentrations were greatest in the SCM, exceeding 200 ng l^{-1} at 45 m. Depth-integrated chl *b* values were also greatest in the STF,
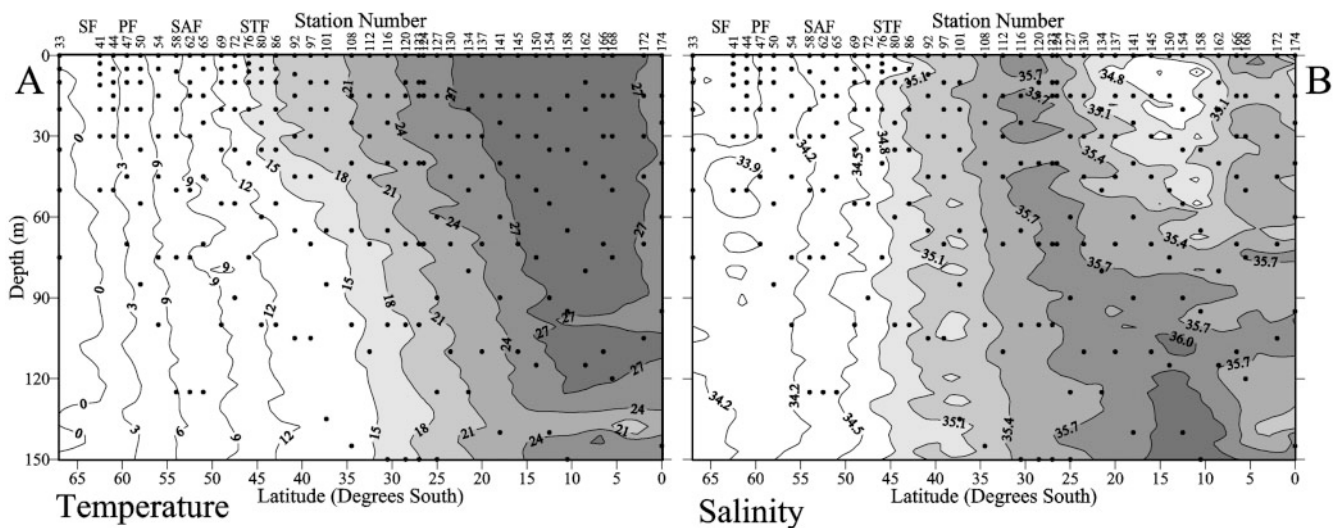

Fig. 2. Transect CTD sections of temperature (°C) and salinity (PSU) down to 150 m. For clarity and comparison, data points indicate location of biological stations sampled on the transect; contour lines shown were plotted from a larger data set that included all CTD stations. Here and in all subsequent figures, stations are labeled as in Fig. 1
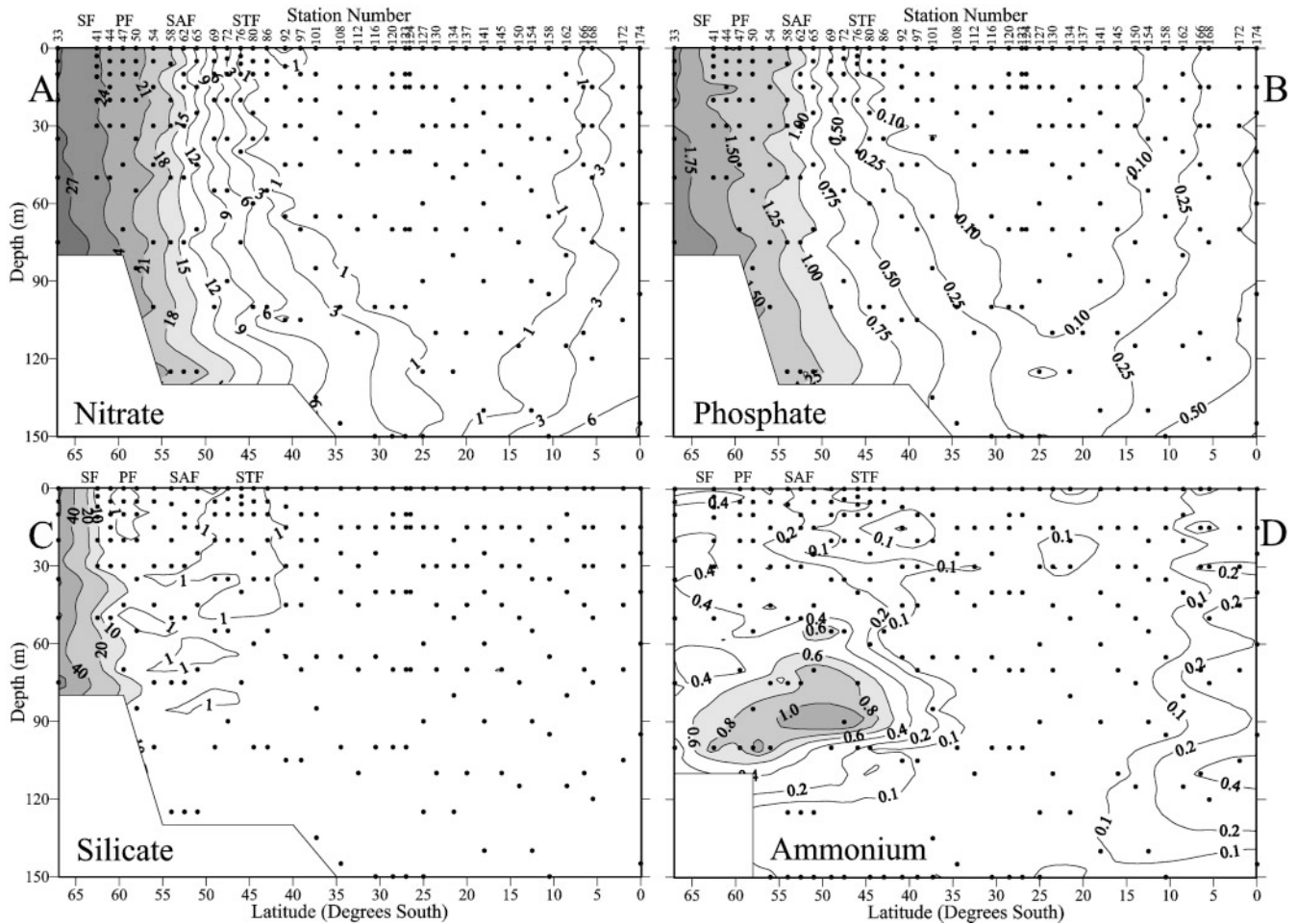
Fig. 3. Nutrient concentration profiles (µM) along sampling transect

with lower values south of the SAZ (Table 4). Total chl *b* concentrations were always greatest in the SCM, and across the SPG concentrations in the SCM were ≥100 ng l⁻¹. In the SPG north of 32° S, there was more total chl *b* below 100 m than above (Table 5). In the EZ, there was more total chl *b* above 100 m than deeper. chl c_1+c_2 concentrations were greatest within and south of the PF, with lesser amounts in the STF and

minor amounts in the SCM of the SPG (Fig. 4C). Depth-integrated amounts of chl c_1+c_2 varied only from 1.1 to 4.6 mg m⁻² across the entire transect (Table 4). Chl c_3 concentrations were greatest in the PF, with a secondary peak in the STF (Fig. 4D), while occurring in the SPG in small amounts concentrated in the SCM. Trends similar to chl c_1+c_2 are apparent in the depth-integrated amounts of chl c_3 (Table 4).

Table 4. Average 0 to 150 m depth-integrated pigment concentrations (mg m⁻²) in each oceanographic zone. Abbreviations as in Table 1

| Zone	Chl *a*	DV chl *a*	Total chl *a*	Total chl *b*	Chl c_1+c_2	Chl c_3	19but	Fucox	19hex	Zeax
AZ	36.782	0.000	36.782	3.373	3.286	4.708	5.185	11.709	8.393	0.443
PF	42.069	0.000	42.069	1.219	4.636	6.946	6.343	9.788	10.921	0.483
PFZ	35.115	0.000	35.115	1.721	3.673	4.399	5.210	8.146	12.427	0.514
SAF	13.197	0.000	13.197	0.779	2.279	1.961	2.938	1.220	15.802	0.192
SAZ	26.070	0.000	26.070	7.470	2.743	2.393	5.579	1.190	20.664	1.448
STF	30.115	1.124	31.239	9.940	3.338	2.460	6.133	1.708	18.588	2.613
SPG	10.871	5.798	16.669	5.914	1.078	0.974	3.123	0.268	5.583	5.848
EZ	10.662	7.571	18.233	5.758	1.071	1.006	3.248	0.315	6.949	6.307
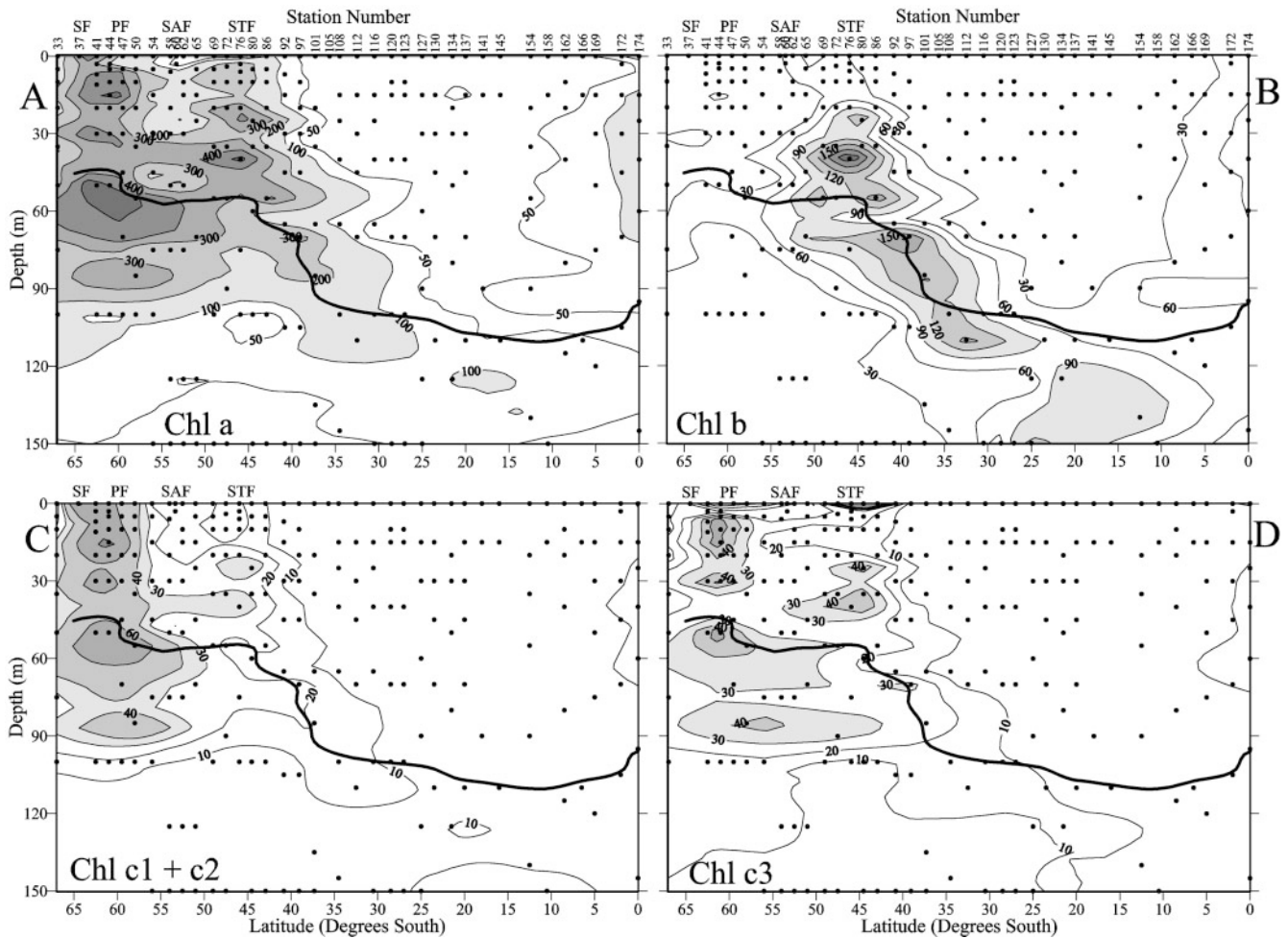
Fig 4. Chlorophyll concentration profiles (ng l^{-1}) along sampling transect. Chl *b* = total chl *b* (i.e. chl *b* + divinyl chl *b*). Here and in all subsequent figures dark contour line in each graph is depth of 1% isolume. See Fig. 13D for divinyl chl *a* profile

Table 5. Pigment ratio averages (±SD) across region from 31°S (Stn 116) to equator (Stn 174). There are 4 stations in each latitudinal range. *Pro*: *Prochlorococcus* spp.; *Syn*: *Synchococcus* spp.; other abbreviations as in Table 1

| Parameter	Depth range	32 to 24°S	24 to 16°S	16 to 8°S	8°S to 0°
DV chl *a*/total chl *a*	0–100 m	0.41 ± 0.04	0.43 ± 0.02	0.52 ± 0.03	0.44 ± 0.05
	101–150 m	0.40 ± 0.08	0.46 ± 0.08	0.50 ± 0.07	0.29 ± 0.15
DV chl *a*/total chl *b*	0–100 m	2.39 ± 1.69	6.74 ± 2.61	8.68 ± 9.35	1.84 ± 0.72
	101–150 m	0.73 ± 0.58	0.78 ± 0.26	1.18 ± 0.66	0.73 ± 0.65
DV chl *a*/zeax	0–100 m	0.52 ± 0.09	0.64 ± 0.07	0.91 ± 0.74	3.02 ± 4.10
	101–150 m	3.09 ± 1.10	2.57 ± 0.17	2.03 ± 0.46	1.64 ± 0.29
DV chl *a*/*Prochl* fg cell^{-1}	0–100 m	0.11 ± 0.03	0.14 ± 0.01	0.17 ± 0.06	0.38 ± 0.13
	101–150 m	1.29 ± 0.51	0.94 ± 0.08	1.18 ± 0.58	0.78 ± 0.67
Integrated chl *a* mg m^{-2}	0–100 m	2.83 ± 0.76	4.62 ± 0.74	4.74 ± 1.60	8.27 ± 2.64
	101–150 m	3.20 ± 1.03	3.19 ± 1.40	3.84 ± 1.54	2.38 ± 0.95
Integrated DV chl *a* mg m^{-2}	0–100 m	1.96 ± 0.47	3.94 ± 0.98	4.95 ± 0.89	6.26 ± 1.31
	101–150 m	2.42 ± 0.45	2.76 ± 1.29	3.90 ± 0.86	1.30 ± 0.89
Integrated total chl *b* mg m^{-2}	0–100 m	0.93 ± 0.60	1.44 ± 0.39	2.69 ± 0.41	4.40 ± 1.77
	101–150 m	3.03 ± 0.87	3.62 ± 1.52	3.37 ± 1.57	1.35 ± 0.59
Integrated *Prochl* 10^{12} cells m^{-2}	0–100 m	18.13 ± 4.30	24.01 ± 2.42	18.23 ± 4.76	15.76 ± 3.25
	101–150 m	6.36 ± 2.57	3.44 ± 1.44	4.11 ± 2.36	2.27 ± 1.11
Integrated *Syn* 10^{12} cells m^{-2}	0–100 m	1.10 ± 0.24	2.88 ± 1.15	3.58 ± 5.13	9.26 ± 2.35
	101–150 m	0.35 ± 0.10	0.16 ± 0.02	0.25 ± 0.16	1.41 ± 0.80
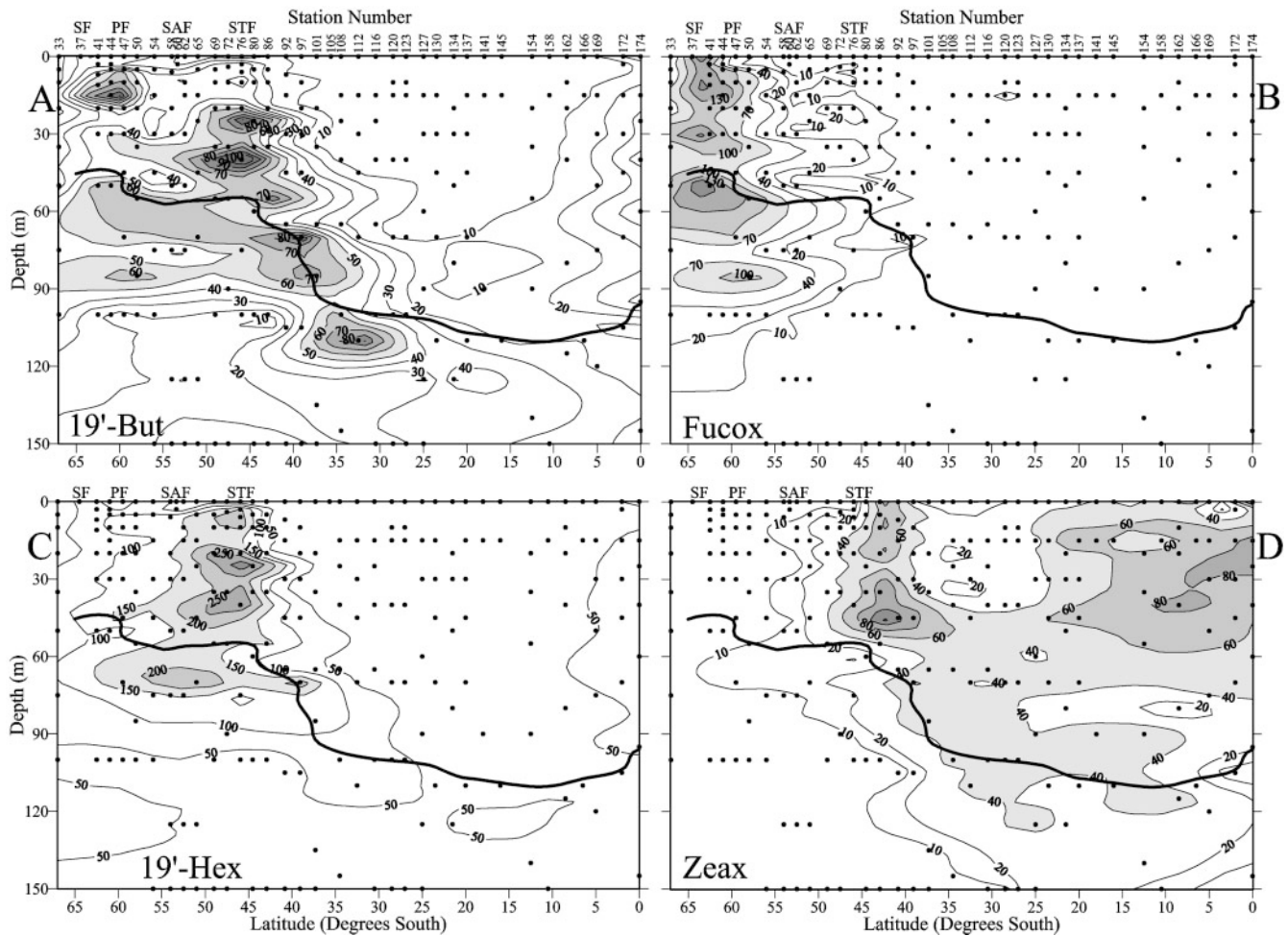
Fig. 5. Major carotenoid concentration profiles (ng l^{-1}) along sampling transect: (A) 19′-butanoyloxyfucoxanthin; (B) fucoxanthin; (C) 19′-hexanoyloxyfucoxanthin; (D) zeaxanthin

Low concentrations of DV chl *a*, found only in *Pro* (Chisholm et al. 1988, Goericke & Repeta 1992), were measured in the STF (Table 4), but only at depth (see Fig. 13D). While maximum DV chl *a* concentrations were found in the SCM of the SPG (with values exceeding 80 ng l^{-1} across the entire region) the depth-integrated values of DV chl *a* showed approximately equal amounts above and below 100 m (Table 5). In contrast, the maximum DV chl *a* concentrations in the EZ was observed in the upper 100 m (see Fig. 13D), resulting in 5-fold higher DV chl *a* concentrations in the upper 100 m than below (Table 5). In the SPG, the DV chl *a*:total chl *a* ratio was ca. 0.45 in both the upper (0 to 100 m) and lower (101 to 150 m) photic zones. In the EZ, the ratio in the upper photic zone was similar (0.44) to that in the SPG, but was only 0.29 in the lower photic zone. The DV chl *a*:total chl *b* ratio in the upper photic zone was greatest in the central and northern part of the SPG, and lower in the southern part of the SPG and in the EZ (Table 5). A lower DV chl *a*:total

chl *b* ratio was observed below 100 m in both the SPG and EZ, similar to laboratory results with *Pro* demonstrating a decrease in this ratio at lowered growth irradiances (Partensky et al. 1993).

Distributions of 3 of the 4 major carotenoids found in these waters, 19but, Fucox, and 19hex, followed a pattern similar to that of the chlorophylls (Fig. 5A–C). Highest concentrations were generally observed in the SF, PF, and STF with a band of elevated concentrations in the SCM across the SPG. The concentration of 19but was greatest in the PF and the STF, exceeding 120 ng l^{-1}. In the SPG, 19but concentrations were greatest in the SCM layer, with low concentrations north of 30° S, primarily in the SCM. There were slightly elevated concentrations (up to 50 ng l^{-1}) of 19but in the EZ. Depth-integrated (0 to 150 m) amounts of 19but were remarkably uniform across the entire transect (Table 4). Fucox concentrations were greatest south of the PF, exceeding 200 ng l^{-1} in some samples. Lower concentrations of Fucox were found in the PF and the SAF

(<100 ng l^{-1}), with little or none found further north in the STF, the SPG, or the EZ. Depth-integrated Fucox amounts were greatest south of the SAF and decreased sharply further north (Table 4). The STF contained the greatest concentrations of 19hex (200 to 300 ng l^{-1}), with lower concentrations further south. The greatest concentration of 19hex was found just north of the STF (380 ng l^{-1}). Decreasing amounts of 19hex were found in the SCM further north, with relatively little or none north of 35° S. Slightly greater concentrations were found in the EZ. Likewise, depth-integrated amounts of 19hex were greatest in the SAZ and STF, with much lower values in the SPG and EZ (Table 4). The distribution of zeaxanthin (zeax) (found primarily in prokaryotic algae) differed markedly from that of the other carotenoids, and was greatest in the southern part of the SPG and in the EZ (Fig. 5D). Unlike all the other pigments, zeax concentrations were not always highest in the SCM. Throughout most of the SPG, zeax was fairly evenly distributed throughout the upper 150 m of the water column with concentrations of 300 to 600 ng l^{-1}. Slightly higher concentrations were found in the EZ, but with a distribution pattern closer to the surface than seen for other pigments. Depth-integrated values for zeax were very low south of the SAZ and increased northward to maximum values in the EZ (Table 4). In the SPG, the ratio of DV chl a:zeax was much lower above 100 m than deeper (Table 5), supporting the hypothesis that zeax serves as a photoprotective agent in prokaryotic algae (Bidigare et al. 1989).

The distribution of phaeopigments was greatest in waters south of STF (65 to 40° S) in conjunction with the dominance of chl c-containing algae. Two major phaeophorbide a peaks ('normal' phaeophorbide a and pyrophaeophorbide a) were observed to elute chro-

matographically between peridinin and Fucox. A third minor peak was also sometimes observed in this region. The sum of the phaeophorbides (Σph-ide) was greatest in the upper 100 m of the water column and revealed several distinct peaks, including one centered at approximately 90 m (Fig. 6A). This Σph-ide peak generally co-varied with the NH_4^+ maximum observed at 90 m throughout the ACC (Fig. 3D); however, there was a distinct latitudinal offset between the maxima in Σph-ide and NH_4^+ concentrations. Chl-ide distributions (Fig. 6B) were very similar to those of Fucox (Fig. 5B) indicating that diatoms were the major taxonomic group containing the chlorophyllase enzyme (Jeffrey & Hallegraeff 1987). Diatom senescence following an earlier bloom would account for this increase in chl-ide (Mengelt et al. 2001). High concentrations of chl-ide will result in an overestimation of chl a when using fluorometric determinations of chl a and may partially explain the overestimation of chl a by fluorometry relative to HPLC chl a separations (Mengelt et al. 2001).

Primary productivity

Peaks in primary production (PP) occurred in the SF and the STF, with rates exceeding 1.0 mg C l^{-1} h^{-1} at the surface (Fig. 7A). The maximum rate of PP was observed in the EZ, where rates exceeded 1.4 mg C l^{-1} h^{-1}. The highest productivity index (g C [g chl]$^{-1}$ h^{-1}) occurred slightly below the surface at 20° S in the SPG (Fig. 7B), where Pro cell numbers were greatest (Fig. 8B). The region of highest PP as well as surface productivity index extended northward into the EZ (Table 6).
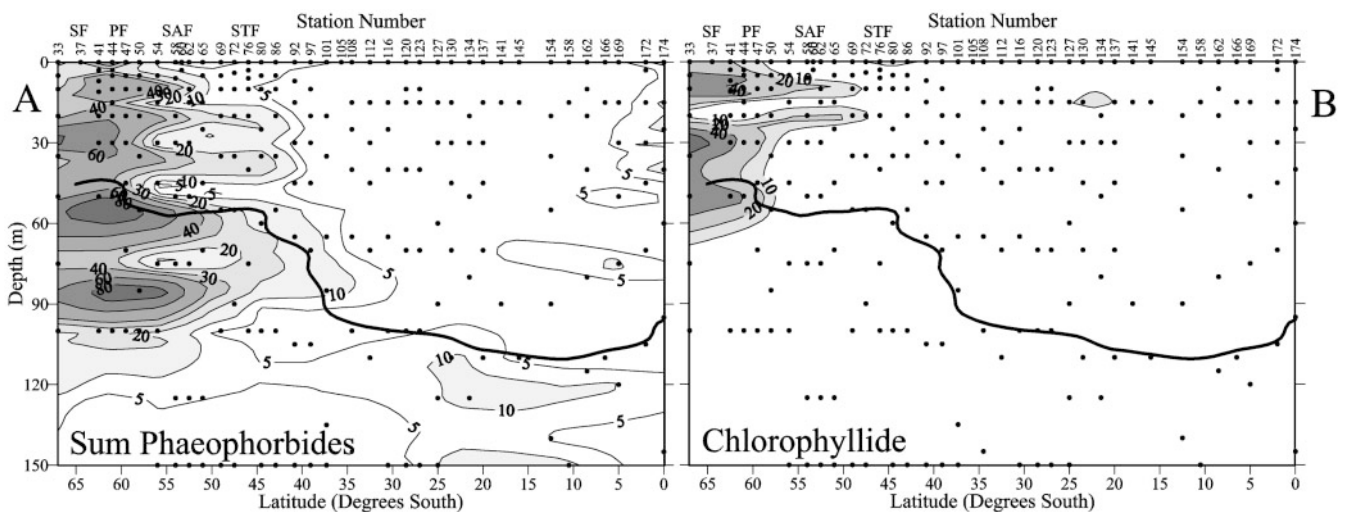

Fig. 6. Phaeopigment concentration profiles (ng l^{-1}) along sampling transect
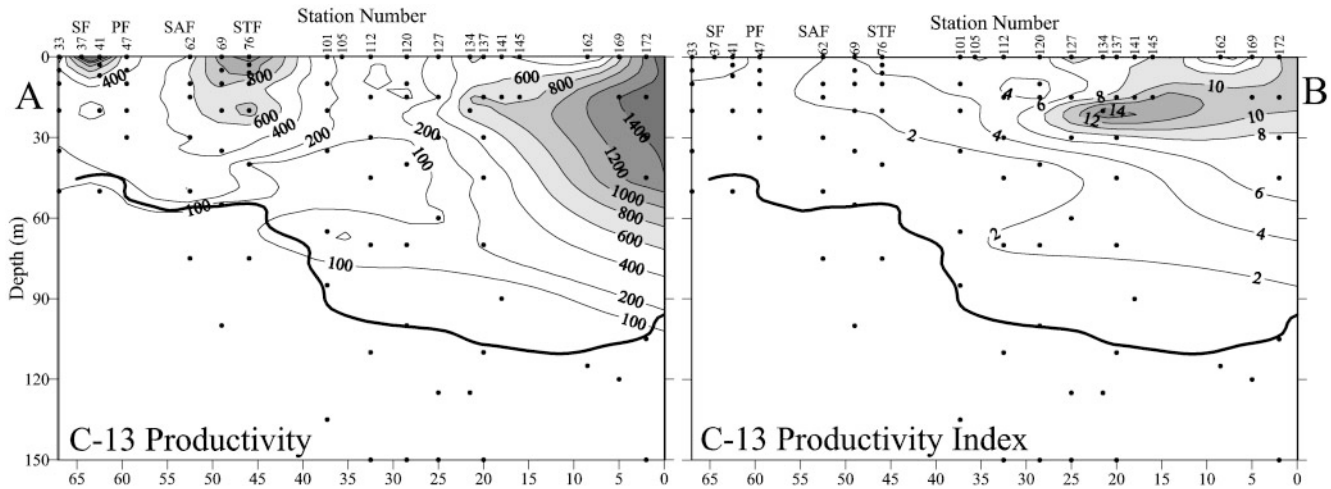
Fig. 7. Productivity along sampling transect. (A) Primary production measured by ^{13}C incorporation (ng C l^{-1} h^{-1}); (B) productivity index (g C g^{-1} chl a h^{-1})

Flow cytometry

Samples for flow cytometry were collected only from Stns 116 (34°S) to 174 (Equator) and counted to determine the abundance of *Syn*, *Pro*, heterotrophic bacteria, and pico-eukaryotic algae (Fig. 8). In the euphotic zone, heterotrophic bacteria were always the most abundant cell type, and were relatively uniform along the transect, ranging between 5×10^5 to 7×10^5 cells ml^{-1} (data not shown), and decreasing below the euphotic zone. *Pro* were the next most abundant group (Fig. 8B) with cell densities ranging up to 2.9×10^5 cells ml^{-1}. *Syn* (Fig. 8A) were more abundant than pico-eukaryotes (Fig. 8C), except at the surface in the EZ, where they were approximately equal. Prokaryotic cells were always greater in surface waters (<50 m) than at depth; however, the latitudinal distribution varied by group. The highest *Syn* cell counts were measured in the EZ, while *Pro* cell counts were highest in the SPG (20 to 25°S). Depth-integrated *Pro* cell counts were 22 and 51% lower in the EZ relative to the SPG above and below 100 m, respectively (Table 5). In conjunction with this decrease in *Pro* abundance, depth-integrated *Syn* cell counts increased by 457 and 267% in the EZ relative to the SPG above and below 100 m, respectively (Table 4). Pico-eukaryotic cell counts were greatest in the surface waters of the EZ, but in the SPG cell counts were slightly greater in the SCM than at the surface.

The ratio of DV chl a:*Pro* cell number increased at depth, especially below the depth of 1% surface irradiance, suggesting that photoacclimation was significant (Fig. 8D). In the SPG, the ratio of DV chl a per cell in the upper 100 m averaged 0.14 fg cell^{-1}, whereas the ratio between the 1% light level (ca. 100 m) and 0.1% light level (ca. 150 m) was nearly 10-fold higher (Table 5). Ratios exceeding 4 fg DV chl a cell^{-1} were observed between 200 and 250 m (data not shown).

CHEMTAX

The results of the CHEMTAX analyses are presented in 2 ways: as a percentage of the total chl a contained in each taxonomic group, and as the amount of chl a or DV chl a contained in each group (Figs. 9 to 13). The first analysis shows the relative contribution of a group to the phytoplankton assemblage at a given location, whereas the second analysis shows the relative biomass distribution of a group along the transect. As previously described, a transition zone existed between 44 and 38°S (Stns 86 to 97), across which the depth of the 1% isolume increased from 60 to 100 m. South of this zone the dominant taxonomic groups were diatoms (Fig. 9A,B),

Table 6. Zonal differences in areal rates of primary production (integrated to depth of euphotic zone) and surface productivity index. N = no. of samples

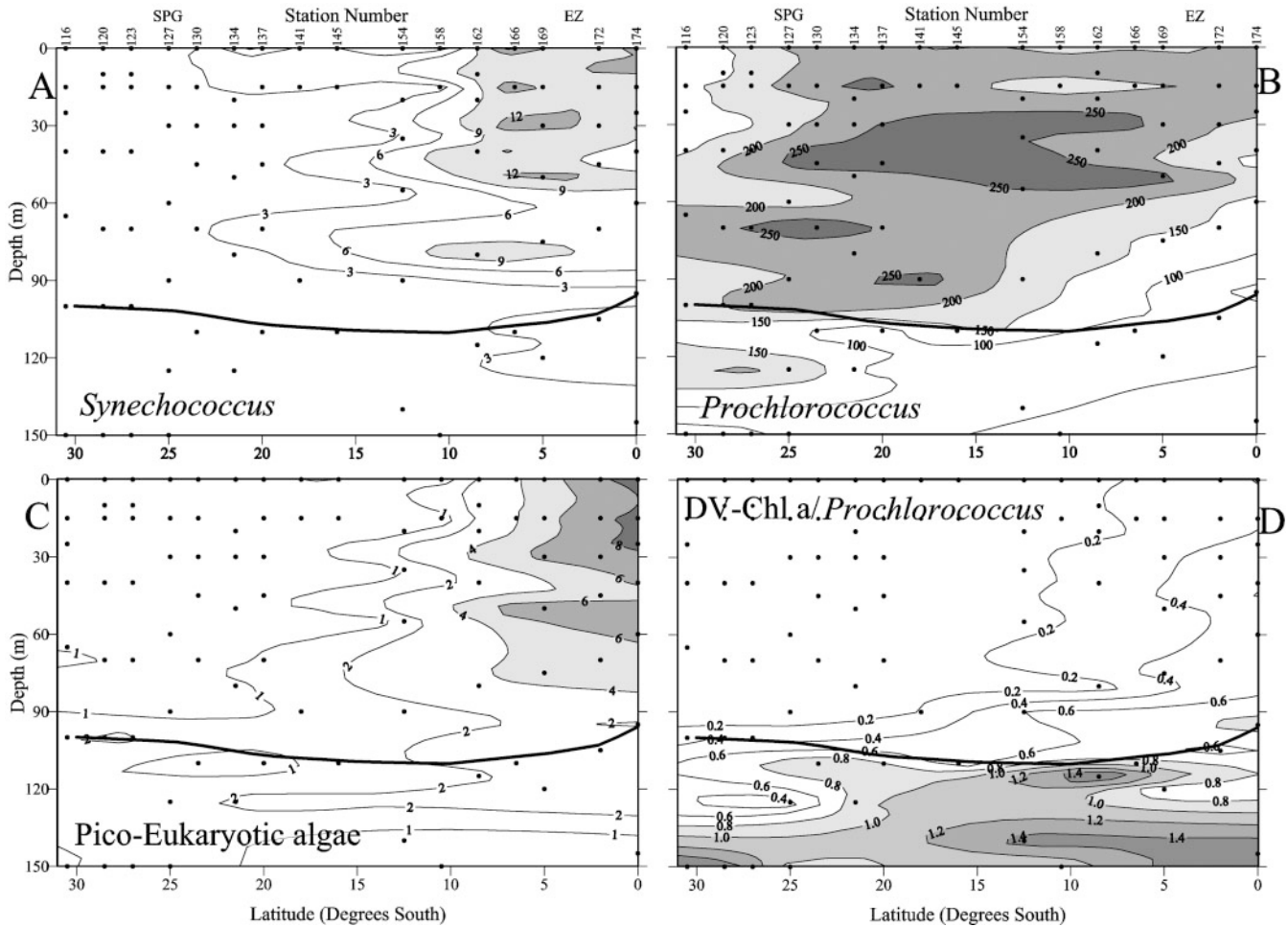| Zone	Station #	N	Primary productivity (g C m^{-2} d^{-1})	Surface productivity index (g C [g total chl a]$^{-1}$ h^{-1})
AZ	33–47	3	0.32 ± 0.10	2.78 ± 2.28
STZ	62–76	3	0.76 ± 0.05	3.59 ± 1.67
SPG	101–162	8	0.58 ± 0.44	5.68 ± 2.60
EZ	169–172	2	2.43 ± 0.23	8.32 ± 5.23

Fig. 8. Cellular abundance profiles (cells × 10^3 ml^{-1}) along portion of sampling transect from 31°S to equator determined by flow cytometry. (A) *Synechococcus* spp.; (B) *Prochlorococcus* spp.; (C) pico-eukaryotic algae; (D) ratio of divinyl chl *a* to *Prochlorococcus* spp. cellular abundance (fg chl cell^{-1}). Note that this figure shows data from SPG (0 to 30°S) only

pelagophytes (Fig. 9C,D), Hapto3 (Fig. 10A,B), Hapto4 (Fig. 10C,D), and chrysophytes (Fig. 11C,D). Cryptophytes (Fig. 11A,B), chlorophytes (Fig. 12A,B) and prasinophytes (Fig. 12C,D) were of lower abundance. North of the transition zone, the phytoplankton assemblage was dominated by *Syn* (Fig. 13A,B), *Pro* (Fig. 13C,D), and Hapto4. Prasinophytes were a minor component of the algal assemblage.

Diatoms contributed significantly to the phytoplankton assemblage only in waters south of the SAF (Fig. 9A,B). Maximum diatom biomass occurred in the surface waters of the ACC between the SF and the SAF down to a depth of 100 m. Diatoms were conspicuously absent at the southernmost station. Pelagophytes were a major portion of the phytoplankton assemblage within and just north of the SAF. Their biomass distribution, however, was bimodal, with a peak in the PF and another in the STF, corresponding with similar peaks in the overall biomass distribution

of chl *a* (Fig. 4A). Pelagophytes had negligible occurrence below the 1% isolume.

Hapto3 comprised greater than 20% of the phytoplankton assemblage only in near-surface waters (<60 m) between the PF and STF, with peak biomass in the STF (Fig. 10A,B). Hapto4 dominated the deep-water phytoplankton assemblage within and south of the STF, but were a negligible component of the surface phytoplankton assemblage (Fig. 10C,D). They had a biomass peak just below the 1% isolume across this region, with biomass exceeding 100 ng chl *a* l^{-1}. Hapto4 accounted for up to 40% of the total chl *a* across the SPG, with slightly greater abundance and biomass in the EZ.

Cryptophytes rarely accounted for more than 20% of the phytoplankton assemblage, but were more than 10% of the assemblage across much of the region within and south of the STF (Fig. 11A,B). Maximum cryptophyte biomass was shallower than the 1% isolume across this region. Chrysophytes dominated the
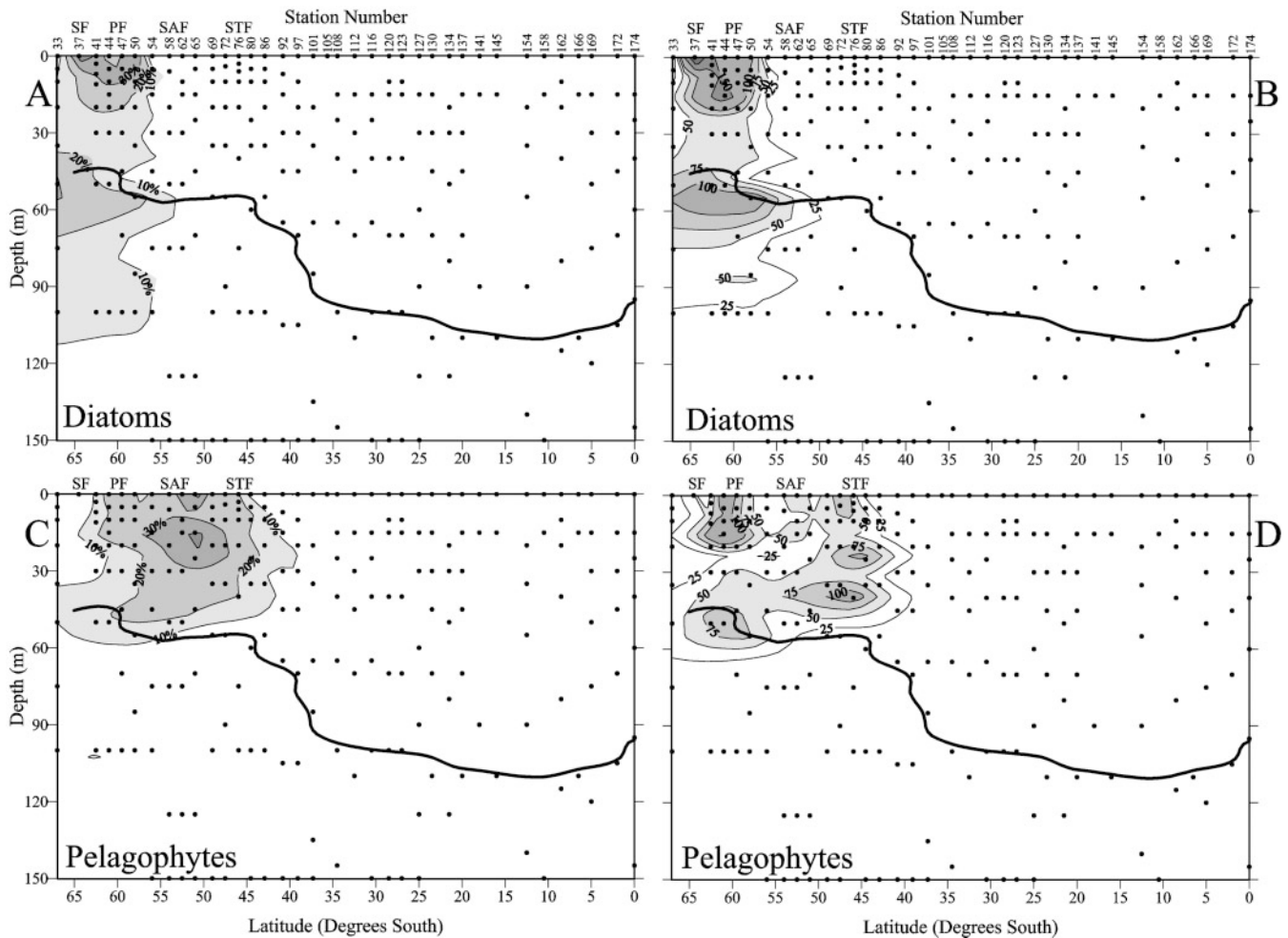
Fig. 9. CHEMTAX analysis results. (A) % total chl *a* in diatoms; (B) chl *a* concentration (ng l^{-1}) in diatoms; (C) % total chl *a* in Pelagophytes; (D) chl *a* concentration (ng l^{-1}) in Pelagophytes

surface phytoplankton assemblage south of the PF, with a secondary peak at 90 m in the PF (Fig. 11C,D).

Chlorophytes were negligible members of the phytoplankton assemblage, always containing less than 5% of the total chl *a* and rarely more than 10 ng chl *a* l^{-1} (Fig. 12 A,B). Prasinophytes were a minor, but consistent, part of the phytoplankton assemblage across much of the transect (Fig. 12C,D). Peak prasinophyte abundance and biomass was in the STF, with a secondary peak in the EZ. Dinoflagellates never contained more than 5% of the total chl *a*, and dinoflagellate biomass was similarly low (<10 ng chl *a* l^{-1}), with a maximum in the PF (data not shown). *Syn* and *Pro* dominated the phytoplankton assemblage in the central part of the SPG (Fig. 13A,C). Both had a biomass maximum in the SCM (Fig. 13B,D), but while peak *Syn* biomass was in the transition zone just north of the STF, *Pro* biomass was greatest in the central SPG with secondary peaks in the transition zone and the EZ.

DISCUSSION

Antarctic zone

Distributions of photosynthetic pigments and cellular abundance during mid-austral summer 1996 revealed distinct differences in the phytoplankton composition that appeared to result from physicochemical differences in the various oceanographic regimes. We observed a great contrast within the AZ between the southernmost station (#33) and the stations north of the SF (#37 to 42). The entire AZ had relatively high macronutrient concentrations (Fig. 3); however, the observed water column stratification at Stn 33 (20 to 30 m: Daly et al. 2001) was shallower than that north of the SF (60 to 70 m). While noon surface irradiance was lower at Stns 33 and 37 (photosynthetically active radiaton, PAR of 280 μE m^{-2} s^{-1}) than at Stn 41 (PAR of 970 μE m^{-2} s^{-1}), these values seem to be above light limitation levels
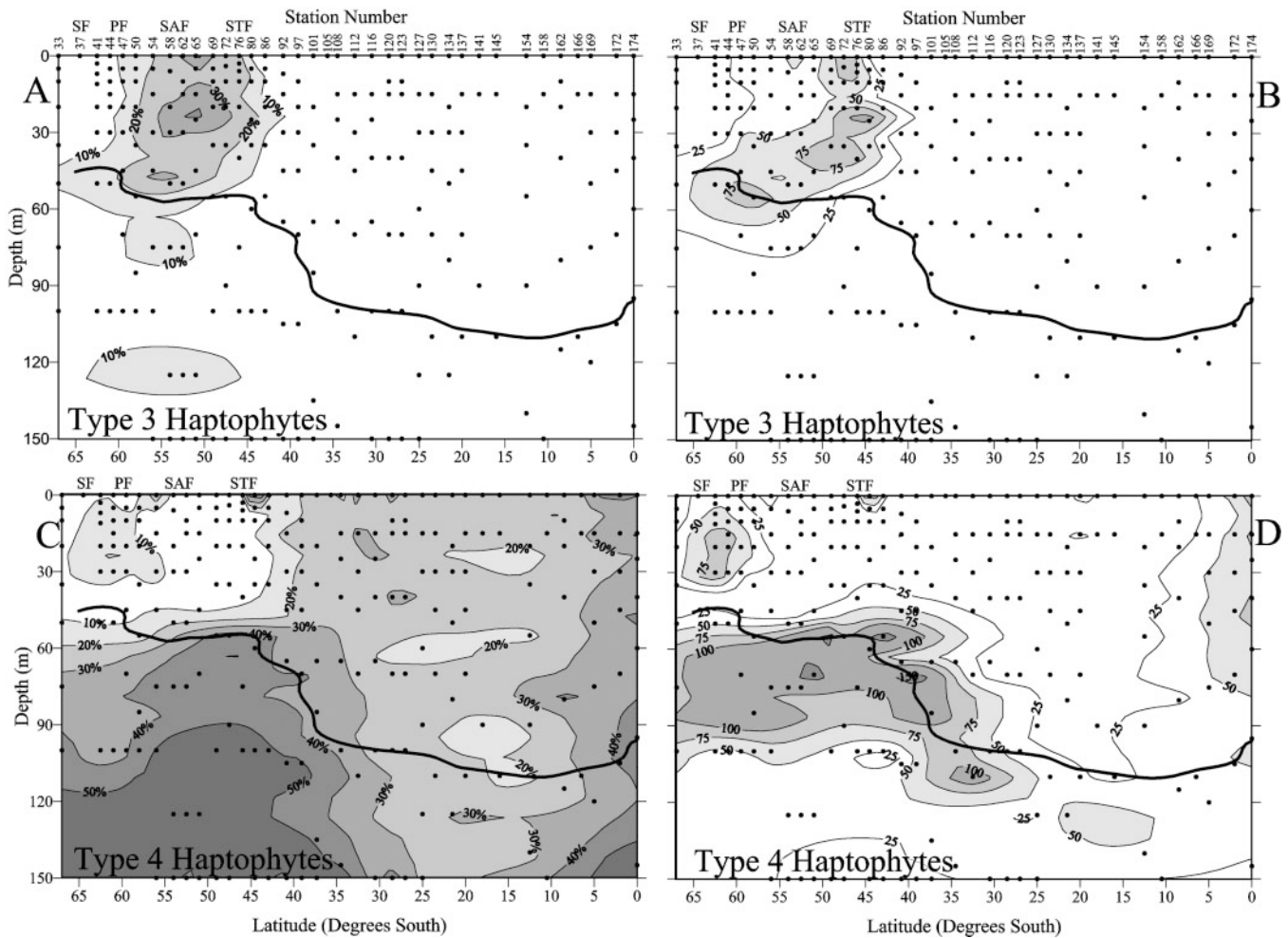
Fig. 10. CHEMTAX analysis results. (A) % total chl *a* in Type 3 haptophytes; (B) chl *a* concentration (ng l^{-1}) in Type 3 haptophytes; (C) % total chl *a* in Type 4 haptophytes; (D) chl *a* concentration (ng l^{-1}) in Type 4 haptophytes

(Mitchell & Holm-Hansen 1991). Mengelt et al. (2001) also concluded that by summer, light-limitation no longer limits phytoplankton growth in this region. Therefore, we would expect to observe higher biomass and productivity at Stn 33 than north of the SF. However, while Stn 33 contained only moderate algal biomass levels (chl *a* <300 ng l^{-1}) and low rates of PP (<400 ngC l^{-1} h^{-1}) at the surface, stations north of the SF had both high biomass (chl *a* > 500 ng l^{-1}) and PP rates (>1000 ngC l^{-1} h^{-1}). In addition to possible light limitation, iron is probably a major factor limiting PP and biomass south of the SF (Martin et al. 1990, Boyd et al. 1995, 1999, Franck et al. 2000, Mengelt et al. 2001), particularly during austral summer. The *in situ* correlation of dissolved iron and algal biomass distribution in the Southern Ocean supports the iron-limitation hypothesis (de Baar et al. 1995, Boyd et al. 1999, 2000, Sedwick et al. 1999, Franck et al. 2000, Mengelt et al. 2001). In the Pacific sector of the Southern Ocean Nolting et al.

(1998) and van Leeuwe et al. (1998b) found lower iron concentrations in the water masses of the AZ than further north, and that the iron that is present may not be bioavailable due to low concentrations of organic complexation compounds (Rue & Bruland 1995). Iron-enrichment experiments conducted by Olson et al. (2000) demonstrated increased photosynthetic efficiency in samples collected from Southern Ocean waters, but not in samples collected from the SF or PF. Van Leeuwe et al. (1998a) determined that prymnesiophytes and diatoms together made up an average of 95% of the total phytoplankton biomass south of the PF. However, they defined prymnesiophytes as all types of algae containing 19hex. We found that the surface phytoplankton assemblage of the AZ consisted primarily of chrysophytes and diatoms, together accounting for nearly 80% of the chl *a*. Hapto4 and pelagophytes, 2 other groups of 19hex-containing algae, accounted for most of the remainder of the chl *a* biomass south of the PF.
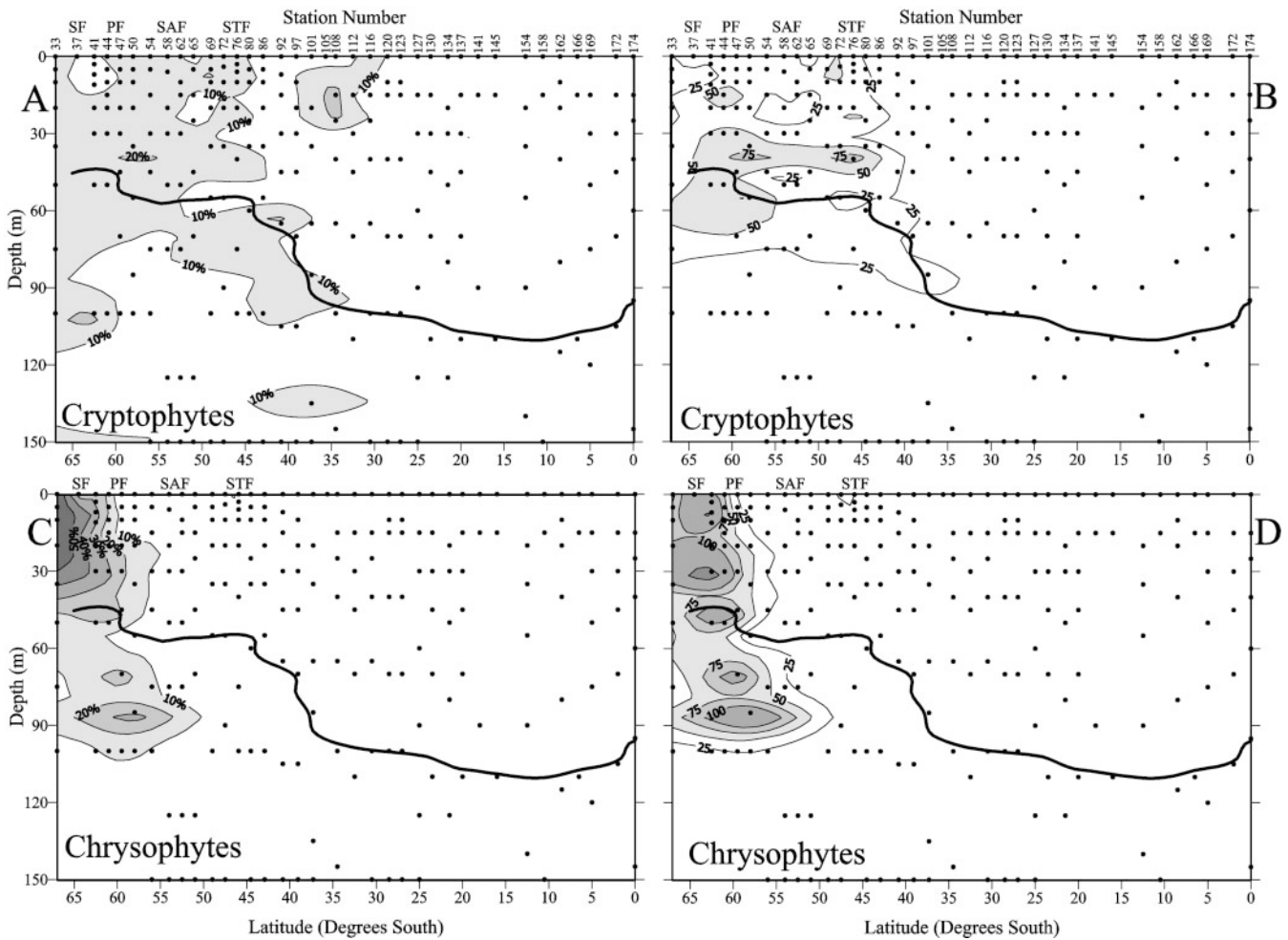
Fig. 11. CHEMTAX analysis results. (A) % total chl *a* in cryptophytes; (B) chl *a* concentration (ng l^{-1}) in cryptophytes; (C) % total chl *a* in chrysophytes; (D) chl *a* concentration (ng l^{-1}) in chrysophytes

Antarctic circumpolar current

The SF and PF are important zones for biological production (Selph et al. 2001). These zones accumulate suspended particulate matter (Bidigare et al. 1996, Nelson et al. 1996, Moore et al. 1999) and the vertical stability maintains a favorable light environment for phytoplankton growth. Stratification was observed at moderate depths (60 to 80 m) between the SF and the PF, and only slightly deeper (about 45 m) than the euphotic zone (Daly et al. 2001). Advection of nutrients into the SF by upwelling maintains high iron and nutrient concentrations favorable for growth (Löscher 1999, Mengelt et al. 2001), but the sinking of biogenic particles rich in silicate will balance this input over seasonal and annual timescales. During the summer, grazing by mesozooplankton can consume up to 21% of the daily phytoplankton production (Urban-Rich et al. 2001). While total chl *a* was about the same in the PF as fur-

ther south, a series of cloudy days with slightly lower irradiance levels (average PAR of 501 ± 221 µE m^{-2} s^{-1} from 63 to 50° S) resulted in a lower PP than in the AZ. The dominance of the phytoplankton assemblage by chrysophytes decreased to less than 20% of the total chl *a* in the PF, with an increase in diatoms, pelagophytes, Hapto3, and Hapto4 (Figs. 9 to 11). While concentrations of nitrate and phosphate remained high across this part of the transect, silicate concentrations decreased markedly (to less than 10 µM), probably as a result of drawdown by the greater abundance of diatoms, but also partly due to meanders and eddies bringing low silicate waters south across the PF.

The ACC region north of the PF was demarcated by extremely low silicate availability (ca. 1 to 3 µM), a function of the southward encroachment of the silicate-limiting zone during the progression of the bloom period (Franck et al. 2000, Nelson et al. 2001). Small, lightly silicified diatoms are predominantly responsi-
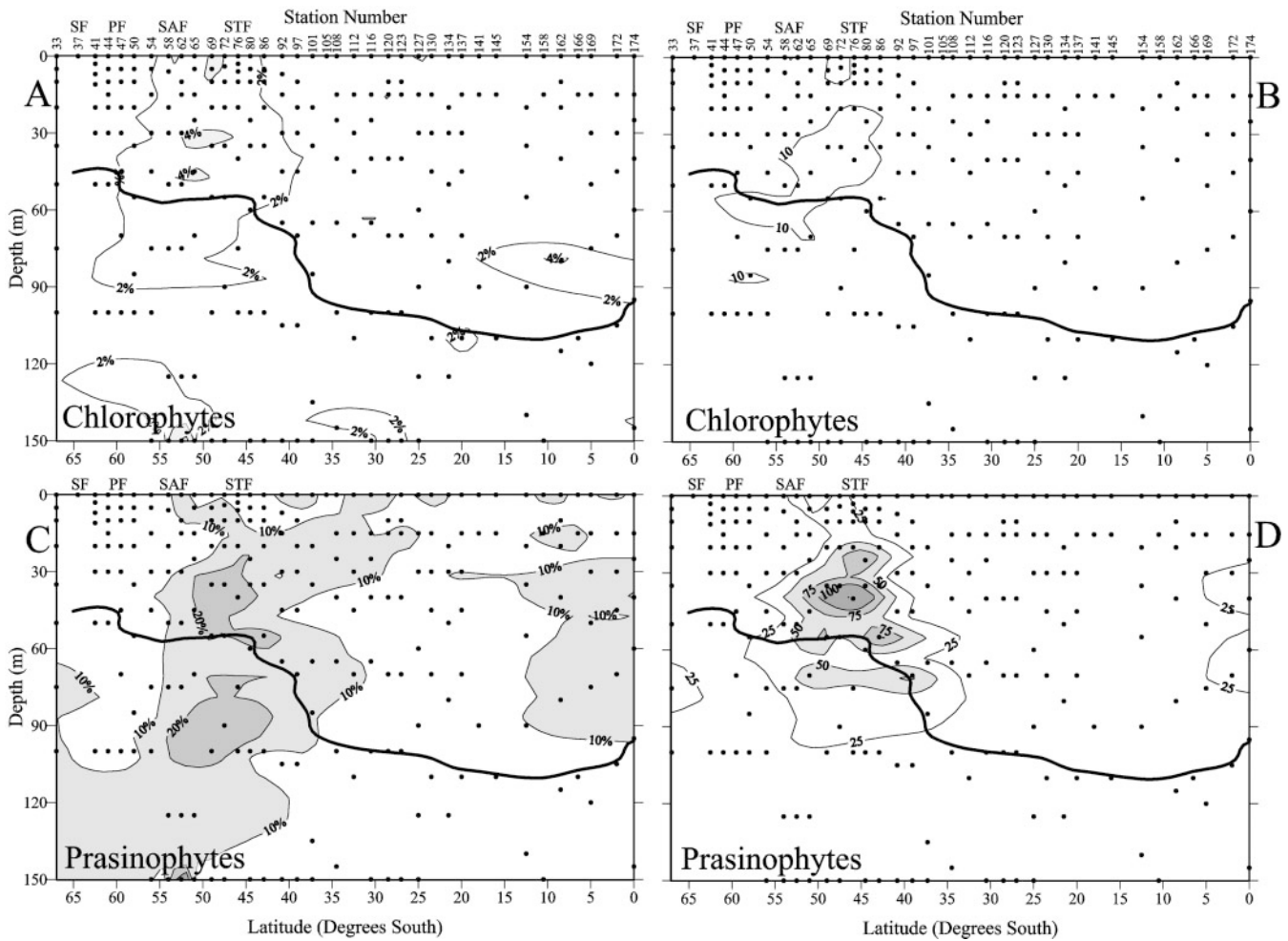
Fig. 12. CHEMTAX analysis results. (A) % total chl *a* in chlorophytes; (B) chl *a* concentration (ng l^{-1}) in chlorophytes; (C) % total chl *a* in prasinophytes; (D) chl *a* concentration (ng l^{-1}) in prasinophytes

ble for the drawdown in silicate concentrations in spring and summer (Hutchins et al. 2001). North of the PF, pelagophytes, Hapto3, and Hapto4 cells continued to increase in biomass and dominance, with a decline in the dominance of diatoms, most probably due to the co-limitation of iron and silicate on diatom growth, especially in the mid- to late-summer period (Nelson & Tréguer 1992, van Leeuwe et al. 1998b, Boyd et al. 1999, de Baar et al. 1999). However, diatoms still represented 10 to 30 % of the total chl *a* in the low-silicate waters between 60 and 55° S. The low concentrations of silicate and the lower abundance of diatoms observed in this region may have resulted from a spring diatom bloom that subsequently sank or was effectively grazed from the surface waters. Within transects across the PF during austral spring (October and November), several studies (Boyd et al. 1995, Peeken 1997, Smith et al. 2000, Nelson et al. 2001) found high silicate concentrations and phytoplankton assemblages

dominated by diatoms. Transects conducted across the PF during summer and fall (January to May) typically find few diatoms and low silicate concentrations (Sullivan et al. 1993, van Leeuwe et al. 1998a, de Baar et al. 1999, Smith et al. 2000, Brown & Landry 2001). During the seasonal progression north of the PF, iron and silicate are probably co-limiting nutrients (Franck et al. 2000). Following the initial diatom bloom, low iron availability can result in enhanced silicate:nitrate uptake ratios for pennate diatoms, leading to a population of thickly silicified cells (Hutchins & Bruland 1998, Takeda 1998, Franck et al. 2000) and a rapid drawdown of silicate concentrations. Even in low-silicate subantarctic waters near Tasmania, lightly silicified pennate diatoms have been observed to proliferate in bottle incubations following iron-addition (Sedwick et al. 1999, Hutchins et al. 2001). Hence, seasonal iron depletion could result in dominance by thickly silicified diatom species during the spring bloom, a transi-
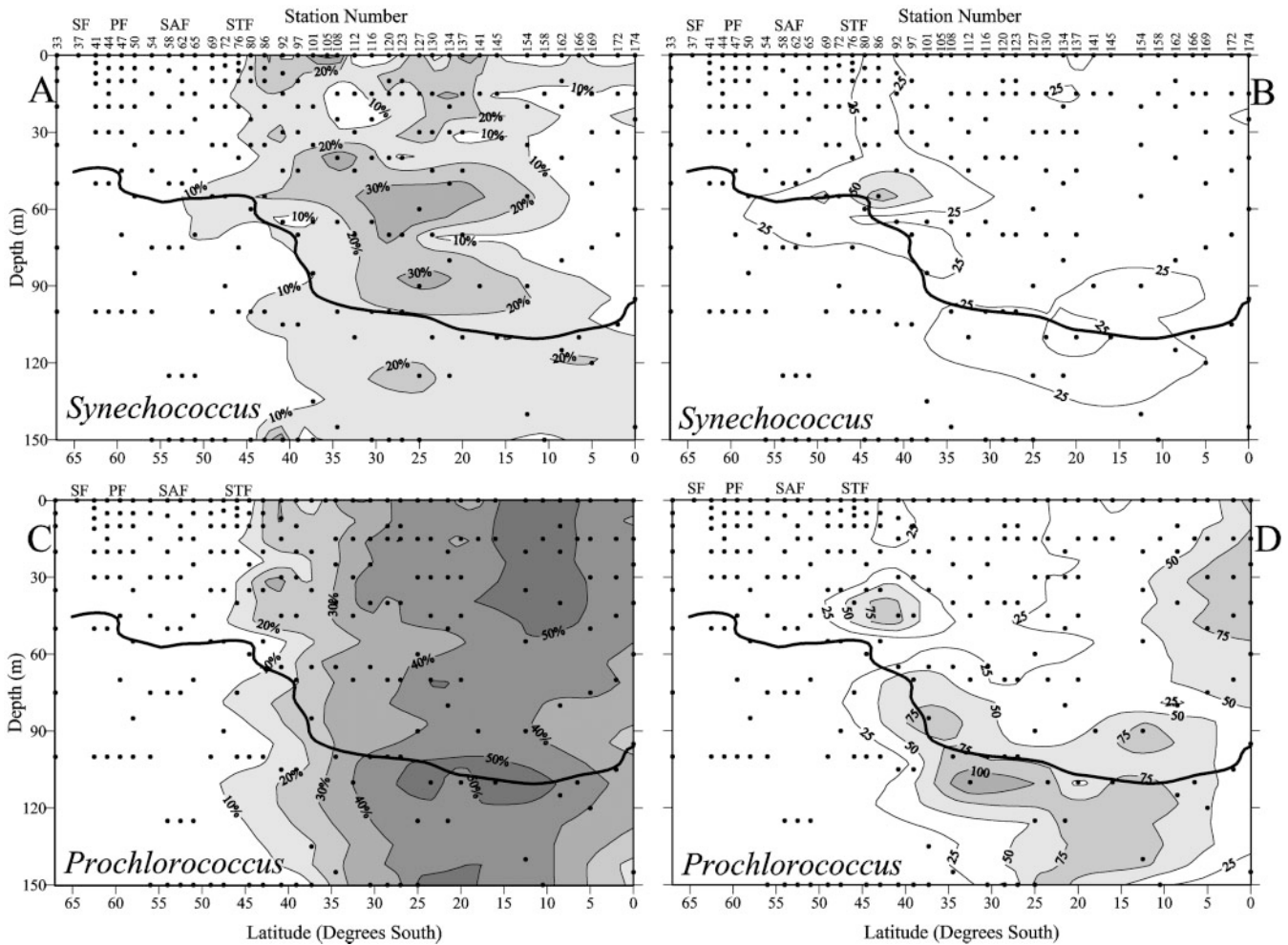
Fig. 13. CHEMTAX analysis results. (A) % total chl *a* in *Synechococcus* spp.; (B) chl *a* concentration (ng l^{-1}) in *Synechococcus* spp.; (C) % total chl *a* in *Prochlorococcus* spp.; (D) divinyl chl *a* concentration (ng l^{-1}) in *Prochlorococcus* spp.

tion to lightly silicified diatoms as silicate becomes limiting, and finally to flagellates when silicate is exhausted during the summer. Other nutrients (nitrate, phosphate, trace metals, etc.) are more rapidly and efficiently recycled by zooplankton grazing (Daly et al. 2001), and are thus not as greatly diminished by the particulate sinking flux.

The distribution of Σph-ide revealed that the most significant processes producing phaeopigments were associated primarily with the region south of the SAF, where the phytoplankton assemblage was dominated by diatoms. Because a mixture of both 'normal' phaeophorbide *a* and pyrophaeophorbide *a* was observed in this region, it is likely that both grazing and senescent processes produced these. Via enhanced settling rates and lowered losses due to mesozooplanktonic grazers and recycling processes, it is possible that diatoms increase the efficiency of the biological pump (Dugdale et al. 1995) compared to smaller phytoplankton

species. However, this may not entirely be the case when iron and silicate are severely co-limiting diatom growth. Under iron limitation, cell size is reduced (Sunda & Huntsman 1997) and smaller diatom species tend to dominate the phytoplankton assemblage (Hutchins et al. 2002). These smaller diatom species may be more susceptible to mesozooplanktonic grazing, which may explain the Σph-ide maximum observed south of the SAF (Fig. 6). Jónasdóttir et al. (1998) suggested that some diatoms inhibit grazing via chemical defense mechanisms, although the effect of individual species on copepod growth and reproduction is poorly known. Ingestion of diatoms by grazers is probably a complex function of species, size, and chemical composition, and our data cannot discern the dominant effect in this region.

The SAF is a region of lower pigment concentrations between the PF and the STF, typical of an HNLC area described by Minas & Minas (1992). Surface geo-

strophic velocities were maximal at the SAF (Daly et al. 2001); this increased the depth of the surface mixed layer to 80 to 100 m, i.e. below the 1% isolume at 60 m. It is conceivable that light limitation could have accounted for the observed low biomass (Mitchell & Holm-Hansen 1991). Hapto3 and pelagophytes dominated the surface phytoplankton assemblage, both in terms of abundance and biomass, even as chl *a* decreased (from >200 to <50 ng l^{-1}) between the PF and the SAF. The abundance and biomass of diatoms decreased sharply along with the decline in silicate concentrations until they accounted for <10% of the total chl *a*. Conversely, the abundance and biomass of the minor components of the assemblage (cryptophytes, chlorophytes, and prasinophytes) continued to increase to the north. For the first time on the transect we observed a SCM at the depth of strong stratification. Pigment concentrations were greater at depths between 30 and 100 m than at the surface, and most groups showed greater chl *a* biomass at these depths than at the surface. Hapto4 cells dominated the phytoplankton assemblage in the SCM.

While blooms of colonial *Phaeocystis antarctica* are generally restricted to the marginal ice zone (El-Sayed & Fryxell 1993, Selph et al. 2001), discounting the prevalence of flagellated *P. antarctica* cells north of the PF may underestimate the true contribution of Hapto4 to total algal biomass, especially near the bottom of the euphotic zone. Although flagellated cells may not be as conspicious as colonial blooms they may be just as important with respect to total biomass as evidenced by the contribution the Hapto4 cells made to the total chl *a* concentration (Fig. 10). Maximum abundance of Hapto4 cells was generally located at depth, with maximum concentrations observed at or below the 1% isolume. Diatom biomass was mostly concentrated at or above the 1% isolume (Fig. 9). A secondary peak below the 1% isolume could be the result of recent sedimentation of a diatom bloom. These trends are consistent with the hypothesis that diatoms flourish in shallow mixed layers while *P. antarctica* populations tend to dominate in regions with deeper mixed layers (Arrigo et al. 1999, 2000).

Subtropical Front

In the STF, PP and phytoplankton chl *a* increased, with little change in the composition of the phytoplankton assemblage. High subsurface (0.5 m) irradiance (1400 µE m^{-2} s^{-1}), strong stratification at shallow depths (20 m and also 60 m, Daly et al. 2001), and low but non-limiting nutrient concentrations probably account for this high PP and biomass. Others (Furuya et al. 1986, Bradford-Grieve et al. 1997, Chang & Gall

1998, Nodder & Gall 1998) have observed similarly high biomass in the convergence zone, but while they have generally observed diatom-dominated phytoplankton assemblages, we observed that flagellates dominated. The difference in the observed assemblage composition probably results from the sampling season: Bradford-Grieve et al. (1997) and Chang & Gall (1998) sampled during the winter and spring, while Furuya et al. (1986) sampled during the early summer. In comparing the phytoplankton assemblage between winter and spring, Chang & Gall (1998) also observed an increase in the relative importance of nanoflagellates in the spring, corresponding to the lower silicate concentrations. Nodder & Gall (1998) observed large fluxes of Fucox and chl *a* in sediment traps during spring, while 19hex and 19but were minor components in the traps. Furuya et al. (1986) postulated that diatoms enter a period of silicate deficiency during or just after their sampling in late December, and that phytoplankton which do not require silicate for growth will eventually dominate the assemblage. This trend of decreasing diatom and increasing flagellate abundance continues into the summer, at which time we found that flagellates completely dominated the assemblage. Hapto3, Hapto4, pelagophytes, and prasinophytes reached their peak abundance and biomass in the STF. Except for the Hapto3, these peaks occurred at depths between 30 and 60 m between the depths of strong stratification (Daly et al. 2001) and coinciding with the SCM. The STF marked the southern limit of *Syn* and *Pro*, which accounted for a small portion of the assemblage.

South Pacific Gyre

Between 44 and 38° S the cruise crossed a transition zone between the STF and the oligotrophic, subtropical waters of the SPG. Across this zone the SCM deepened from 50 to 90 m (Fig. 4A), the depth of the 1% isolume deepened from 60 to 100 m, and the surface phytoplankton assemblage shifted from a eukaryotic-dominated system in the STF to a prokaryotic-dominated system in the SPG. A vertical separation of phytoplankton assemblages occurred within this transition zone, continuing into the SPG, with prokaryotes dominating the surface assemblage and eukaryotes (Hapto4, cryptophytes, and prasinophytes) dominating the assemblage in the SCM.

Surface waters of the SPG are highly oligotrophic, with most nutrient concentrations at or below detection limits. Iron limitation is widespread across this region (Behrenfeld & Kolber 1999). These waters were dominated by prokaryotic algae and contained relatively low eukaryotic algal biomass. Hapto4 and prasinophytes

comprised a minor portion of the assemblage (<30%). *Pro* dominated the surface assemblage both in terms of total chl *a* biomass and numerically, based on the flow cytometry results, while *Syn* ranked second. In contrast, Mackey et al. (1998), using CHEMTAX to analyze the pigment distribution in the western tropical Pacific, concluded that *Syn* dominated the chl biomass in surface waters and *Pro* was of secondary importance. In the same region, Shimada et al. (1993) reported that *Pro* dominated numerically over *Syn* in surface waters; however, they observed greater *Syn* cell numbers in the SCM than in surface waters, while we observed lower *Syn* cell numbers in the SCM (Fig. 8). Claustre et al. (1999), measuring cellular fluorescence, described the surface waters as being dominated by *Pro* and pico-eukaryotes, with *Syn* of secondary importance. Consistent with our observations, all these reports described dominance by *Pro* in the SCM.

Across the SPG, north of this transition zone, the SCM continued to deepen, reaching a maximum of 130 m at 20° S, corresponding to the axis of the gyre circulation (Stramma et al. 1995). The SCM consistently fell within the nitracline, and closely followed both the 1% isolume and the 1 μM NO_3^- contour line. Similarly, Blanchot et al. (1992) located the SCM along the 0.1 μM NO_3^- contour. Physically, the SPG conforms to the typical tropical structure as described by Blanchot & Rodier (1996), with a 2-layered structure separated by a strong pycnocline. There was a distinct difference in phytoplankton composition between surface waters (<100 m) and the SCM. This separation of assemblages is consistent with numerous other observations linking the phytoplankton assemblage composition with nutrient levels: small prokaryotic algae dominate in near-surface, nutrient-depleted, high-light environments, while pico-eukaryotes dominate in the deeper, higher nutrient, low-light environment of the SCM (Blanchot et al. 1992, Le Bouteiller et al. 1992, Blanchot & Rodier 1996). Le Bouteiller et al. (1992) reported that phytoplankton biomass in low-nutrient surface water was mostly in the <1 μm size fraction, while in the SCM the >1 μm size fraction contained the majority of the biomass. Based on our CHEMTAX results, eukaryotic algae (Hapto4, cryptophytes, and prasinophytes) contributed significantly to the assemblage in the SCM, comprising about 50% of the assemblage, but only Hapto4 were found across the entire SPG. *Pro* distributions, as indicated by DV chl *a* concentrations, tracked the 1% isolume (Fig. 13D) and, more closely, the 1 μM nitrate contour (Fig. 3A). Whether these relationships are cause and effect is not clear; however, Olson et al. (1990) in the North Atlantic Ocean and Shimada et al. (1993) in the West Pacific also related *Pro* distributions to the position of the nitracline. Pico-eukaryotes, which showed maximal concentrations at the top of the nitracline, were probably fueled by nitrate diffusion across the pycnocline leading to 'new' primary production at this depth.

Photoacclimation is an important process in the SPG. Cellular fluorescence increases with depth in all groups of algae (Blanchot & Rodier 1996). For prokaryotes, photoacclimation to the light levels throughout the water column is of high significance. In the high-light surface waters, *Syn* have been shown to acclimate by synthesizing more of the photoprotective pigment zeax and accessory light-harvesting pigments such as phycoerythrin and phycocyanin (Olson et al. 1988, Bidigare et al. 1989). In deeper, more light-limited waters, *Syn* produce more chl *a* per cell (Blanchot & Rodier 1996). Similarly, *Pro* photoacclimate to lower light levels by increasing their cellular DV chl *a* content (Partensky et al. 1993, Blanchot et al. 2001). Cellular fluorescence of surface *Pro* can be so weak that they are difficult to enumerate (Claustre et al. 1999). Shimada et al. (1993) reported a 10-fold greater fluorescence per cell at the depth of the 1% isolume than at the surface. We observed that the cellular DV chl *a* concentration was 5 times greater at the depth of the 1% isolume relative to that at the surface (Fig. 8D). Similarly, the results from the CHEMTAX analysis by Mackey et al. (1998) showed a >10-fold increase in the chl *a*:zeax ratio for prochlorophytes between the surface depth bin (1) and the deepest depth bin (12). We also observed a significantly higher ratio (4-fold) in deeper water (101 to 150 m) than in shallower water (0 to 100 m) (Table 5).

Below the 1% isolume, the nitracline, and the SCM, pigment concentrations, cell numbers, and productivity decreased markedly, but not all pigments and cell numbers declined at the same rate; DV chl *a* and *Pro* cell numbers decreased to a lesser extent than others. *Pro* cells that dominated this very deep environment were highly photoacclimated with very high cellular DV chl *a* content (1 to 4 fg cell^{-1}). This huge difference in cellular DV chl *a* can be attributed to 2 subpopulations of *Pro*, 1 at the surface adapted to high-light and 1 in deep water adapted to low-light (Campbell et al. 1994, Blanchot & Rodier 1996, Moore et al. 1998, Blanchot et al. 2001). Goericke et al. (2000) reported finding a novel *Prochlorococcus* species in low-light, suboxic environments of the Eastern Tropical Pacific and Arabian Sea that contained a unique complement of photosynthetic pigments including parasiloxanthin. These populations formed near monoalgal cultures at some locations and depths, often below the euphotic zone. No samples in this survey contained parasiloxanthin. Moore et al. (1998) determined that surface and deep populations of *Pro* in the North Atlantic Ocean are closely related, yet genetically different, ecotypes, physiologically adapted to their respective nutrient and light environments.

Equatorial Zone

North of 10° S the cruise entered the EZ, a region of equatorial upwelling with hydrographic conditions consistent with non-El Niño periods (Ishizaka et al. 1997). In fact, this cruise took place at the beginning of a La Niña event (Le Borgne et al. 1999). This HNLC regime is distinct from both the SPG and the oligotrophic warm pool of the western Equatorial Pacific (Blanchot et al. 2001) by having a shallow and dispersed SCM, elevated macronutrient (NO_3^-, PO_4^-, NH_4^+) concentrations, a shallower euphotic zone, and slightly higher pigment concentrations. Consistent with other reports (Iriarte & Fryxell 1995, Raimbault et al. 1999, Blanchot et al. 2001), a surface mixed layer of 60 to 90 m depth, slightly shallower than the euphotic zone, is generally distinguished from deeper waters and contains the majority of the phytoplankton cell numbers and biomass (Chavez et al. 1990, Le Bouteiller et al. 1992, Kaczmarska & Fryxell 1995, André et al. 1999, Blanchot et al. 2001). In this region, surface ^{13}C PP was comparable to values observed in the STF, where nutrient concentrations were similar but not as great as would be expected in a tropical environment. Our average surface productivity indices (8 g C [g total chl a]$^{-1}$ h^{-1}) in the EZ were similar to those measured (photosynthesis–irradiance [P–I] values of 5 to 6) in February and March, 1988 along 150° W (Cullen et al. 1992). Our P–I values, however, were significantly lower than those measured in other warm waters (>26°C) with reported P–I values as high as 20 to 25 g C (g total chl a)$^{-1}$ h^{-1} (Malone & Neale 1981, Falkowski 1983). The lower P–I values in our study and that of Cullen et al. (1992) probably reflect the effects of nutrient limitation on phytoplankton growth in the EZ. Photosynthesis versus irradiance measurements in this region also indicated that nutrient limitation was important despite elevated NO_3^- concentrations (Lindley et al. 1995). As in other HNLC environments, iron is probably the limiting factor for phytoplankton growth (Martin 1992, Lindley et al. 1995, Hoge et al. 1998, Raimbault et al. 1999); however, silicate may also act as a co-limiting nutrient (Dugdale & Wilkerson 1998). Elevated concentrations of NH_4^+ in the EZ support the idea that regenerated production is an important process, which retards the drawdown of nitrate levels (Wilkerson & Dugdale 1992, Raimbault et al. 1999).

Compared to the SPG, *Pro* cell numbers in surface waters of the EZ were slightly lower, but were still 1 order of magnitude greater than *Syn* or pico-eukaryotes. Although *Pro* cell numbers were less, a greater cellular quota of DV chl a (Fig. 8D, Table 5) resulted in greater chl a biomass here than in the SPG (Fig. 13D), so they still accounted for nearly half (44%) of the total chl a biomass (Table 5). Ishizaka et al. (1997) reported 30% of the total chl as DV chl a. The relative dominance of *Pro* in the EZ varies longitudinally and temporally (Iriarte & Fryxell 1995, Suzuki et al. 1997). The shift in abundance and distribution between El Niño and non-El Niño periods can be quite important (Blanchot et al. 1992, Bidigare & Ondrusek 1996, Blanchot & Rodier 1996, Ishizaka et al. 1997, Higgins & Mackey 2000). While Chavez et al. (1990) reported dominance in the surface layer by *Syn*, other authors have reported dominance of the surface layer by *Pro* (Blanchot & Rodier 1996, André et al. 1999, Blanchot et al. 2001) or by eukaryotes (Le Bouteiller et al. 1992, Claustre et al. 1999). Generally, the surface phytoplankton assemblage in this HNLC region is a diverse community of prokaryotic and eukaryotic algae.

In our survey, Hapto4 and prasinophytes together accounted for about 45% of the total chl a biomass in the surface zone, with *Syn* contributing only about 10%, consistent with the results of other surveys in the region (Bidigare & Ondrusek 1996, Mackey et al. 1998, Moon-van der Staay et al. 2000, Blanchot et al. 2001). Numbers of pico-eukaryotes increased from <1000 cells ml^{-1} in the SPG to >8000 cells ml^{-1} in the EZ, and *Syn* cell numbers also increased from <3000 to >9000 cells ml^{-1}.

Below the surface mixed layer and the euphotic zone, pigment concentrations and cell numbers decreased markedly. As in the SPG, a low-light-adapted ecotype of *Pro* occurred in this deep-water layer (Blanchot et al. 2001). The relative contribution of *Pro* was, however, lower than in the surface layer (<30% of the total chl; Table 5), while Hapto4 contained >40% of the total chl and *Syn* accounted for another 10 to 20%. This observation that pico-eukaryotes dominated the phytoplankton assemblage biomass in deep water was consistent with previous reports (Satoh et al. 1992, Blanchot & Rodier 1996, Claustre et al. 1999, Blanchot et al. 2001), however, the greater importance of *Syn* at depth contradicted these reports.

CHEMTAX

The analysis of HPLC pigments by CHEMTAX is an innovative method for determining the composition of a mixed phytoplankton assemblage. Previous attempts have relied on equations using only a few diagnostic pigments to determine the relative abundance of a limited number of phytoplankton groups (Letelier et al. 1993, Tester et al. 1995, Bidigare & Ondrusek 1996). While suitable for a limited number of samples collected from a fairly uniform environment, these earlier analyses were unable to account for changes in pigment ratios that may occur due to environmental changes (e.g. light levels) or major shifts in the phyto-

plankton assemblage between ecosystems. Because CHEMTAX calculates a single final pigment ratio matrix for the entire data set being analyzed, the analysis of a large set of samples must have the sample set broken up into discrete sets based on environmental parameters for separate analyses. Expecting variations in the pigment ratios within each algal group due to photoacclimation and taxonomic changes between ecosystems, we chose to divide our large sample set (270 samples) into 7 depth bins and 2 latitudinal sections for 14 separate analyses. There is no need, however, for the user to absolutely define the pigment-ratio matrix for each analysis beforehand. Instead, CHEMTAX allows the user-defined initial pigment-ratio matrix to shift during the analysis based on a continual comparison of the pigment-ratio matrix to the data set. This allows the user some latitude in defining the initial pigment-ratio matrix. While it is best for the user to create the most accurate initial pigment-ratio matrix possible in order to calculate the phytoplankton assemblage composition, CHEMTAX is tolerant of random variations in the initial pigment ratio matrix as well as in the pigment-data matrix (Mackey et al. 1997). Subtle variations in pigment ratios due to light, nutrient, or other environmental parameters have only a minor impact on the CHEMTAX biomass calculations (Schlüter et al. 2000), and CHEMTAX analyses of pigment concentrations often have high correlations with microscopic enumeration (Lampert et al. 2000). At very low pigment concentrations, where small inaccuracies in determining the pigment concentrations can result in significantly large changes in pigment ratios, CHEMTAX has problems distinguishing between algal groups with similar suites of pigments (e.g. Hapto3 and Hapto4). In our analyses this was especially apparent in samples collected from deep waters (>150 m) and from the surface waters of the SPG. This problem can be partially offset by more accurately defining the initial pigment-ratio matrix.

CONCLUSIONS

Our results documented the large-scale distributional patterns of phytoplankton biomass, assemblage composition, and productivity in the South Pacific Ocean. Differences in both algal abundance and productivity rates were not unexpected, given the wide range in environmental factors that control and influence both. Such environmental variables also are expected to change over time, and the associated biogeochemical processes will undoubtedly be altered. Knowledge of the broad basin-wide pattern of phytoplankton distribution is a first step in the assessment of these long-term trends.

LITERATURE CITED

André JM, Navarette C, Blanchot J, Radenac MH (1999) Pico-phytoplankton dynamics in the equatorial Pacific: growth and grazing rates from cytometric counts. J Geophys Res 104:3369–3380

Arrigo KR, Robinson DH, Worthen DL, Dunbar RB, DiTullio GR, Van Woert M, Lizotte MP (1999) Phytoplankton community structure and the drawdown of nutrients and CO_2 in the Southern Ocean. Science 283:365–367

Arrigo KR, DiTullio GR, Dunbar RB, Robinson DH, Van Woert M, Worthen DL, Lizotte MP (2000) Phytoplankton taxonomic variability in nutrient utilization and primary production in the Ross Sea. J Geophys Res 105:8827–8846

Behrenfeld MJ, Kolber ZS (1999) Widespread iron limitation of phytoplankton in the South Pacific Ocean. Science 283: 840–843

Bidigare RR, Ondrusek ME (1996) Spatial and temporal variability of phytoplankton pigment distributions in the Central Equatorial Pacific Ocean. Deep-Sea Res II 43:809–833

Bidigare RR, Schofield O, Prézelin BB (1989) Influence of zeaxanthin on quantum yield of photosynthesis of *Synechococcus* clone WH7803. Mar Ecol Prog Ser 56:177–188

Bidigare RR, Iriarte JL, Kang SH, Karentz D, Ondrusek ME, Fryxell GA (1996) Phytoplankton: quantitative and qualitative assessments: foundations for ecological research west of the Antarctic Peninsula. Antarct Res Ser 70: 173–198

Blanchot J, André JM, Navarette C, Neveux J, Radenac MH (2001) Picophytoplankton in the equatorial Pacific: vertical distributions in the warm pool and in the high nutrient low chlorophyll conditions. Deep-Sea Res I 48:297–314

Blanchot J, Rodier M (1996) Picophytoplankton abundance and biomass in the western tropical Pacific Ocean during the 1992 El Niño year: results from flow cytometry. Deep-Sea Res II 43:877–895

Blanchot J, Rodier M, Le Bouteiller AL (1992) Effect of El Niño Southern Oscillation events on the distribution and abundance of phytoplankton in the Western Pacific Tropical Ocean along 165° E. J Plankton Res 14:137–156

Boyd P, LaRoche J, Gall M, Frew R, McKay RML (1999) Role of iron, light, and silicate in controlling algal biomass in subantarctic waters SE of New Zealand. J Geophys Res 104:13395–13408

Boyd P, Watson AJ, Law CS, Abraham ER and 30 others (2000) A mesoscale phytoplankton bloom in the polar

Southern Ocean stimulated by iron fertilization. Nature 407:695–702

Boyd PW, Newton (1999) Does planktonic community structure determine downward particulate organic carbon flux in different oceanic provinces? Deep-Sea Res 46:63–92

Boyd PW, Robinson C, Savidge G, Williams PJ, Le B (1995) Water column and sea-ice primary production during Austral spring in the Bellinghausen Sea. Deep-Sea Res II 42: 1177–1200

Bradford-Grieve JM, Chang FH, Gall M, Pickmere S, Richards F (1997) Size-fractioned phytoplankton standing stocks and primary production during austral winter and spring 1993 in the Subtropical Convergence region near New Zealand. NZ J Mar Freshw Res 31:201–224

Brown SL, Landry MR (2001) Microbial community structure and biomass in surface waters during a Polar Front summer bloom along 170°W. Deep-Sea Res II 48:4039–4058

Campbell L, Vaulot D (1993) Photosynthetic picoplankton community structure in the subtropical North Pacific ocean near Hawaii (Station ALOHA). Deep-Sea Res 40: 2043–2060

Campbell L, Nolla HA, Vaulot D (1994) The importance of *Prochlorococcus* to community structure in the central North Pacific Ocean. Limnol Oceanogr 39:954–961

Chang FH, Gall M (1998) Phytoplankton assemblages and photosynthetic pigments during winter and spring in the Subtropical Convergence region near New Zealand. NZ J Mar Freshw Res 32:515–530

Chavez FP, Buck KR, Barber RT (1990) Phytoplankton taxa in relation to primary production in the equatorial Pacific. Deep-Sea Res 37:1733–1752

Chisholm SW, Olson RJ, Zettler ER, Goericke R, Waterbury JB, Welschmeyer NA (1988) A novel free-living prochlorophyte abundant in the oceanic euphotic zone. Nature 334: 340–343

Claustre H, Morel A, Babin M, Cailliau C, Marie D, Marty JC, Tailliez D, Vaulot D (1999) Variability in particle attenuation and chlorophyll fluorescence in the tropical Pacific: scales, patterns, and biogeochemical implications. J Geophys Res 104:3401–3422

Cooper DJ, Watson AJ, Nightingale PD (1996) Large decrease in ocean-surface CO_2 fugacity in response to *in situ* iron fertilization. Nature 383:511–513

Cullen JJ, Lewis MR, Davis CO, Barber RT (1992) Photosynthetic characteristics and estimated growth rates indicate grazing is the proximate control of primary production in the Equatorial Pacific. J Geophys Res 97:639–654

Daly KL, Smith WO Jr, Johnson GC, DiTullio GR and 5 others (2001) Hydrography, nutrients, and carbon pools in the Pacific sector of the Southern Ocean: implications for carbon flux. J Geophys Res 106:7107–7124

de Baar HJW, de Jong JTM, Bakker DCE, Löscher BM, Veth C, Bathmann U, Smetacek V (1995) Importance of iron for plankton blooms and carbon dioxide drawdown in the Southern Ocean. Nature 373:412–415

de Baar HJW, de Jong JTM, Nolting RF, Timmermans KR, van Leeuwe MA, Bathmann U, Rutgers van der Loeff MM, Sildam J (1999) Low dissolved Fe and the absence of diatom blooms in remote Pacific waters of the Southern Ocean. Mar Chem 66:1–34

DiTullio GR, Geesey ME (2002) Photosynthetic pigments in marine algae and bacteria. In: Bitton G (ed) The encyclopedia of environmental microbiology. John Wiley & Sons, New York, p 2453–2470

DiTullio GR, Laws EA (1991) Impact of an atmospheric–oceanic disturbance on phytoplankton community dynamics in the North Pacific Central Gyre. Deep-Sea Res 38:1305–1329

DiTullio GR, Hutchins DA, Bruland KW (1993) Interaction of iron and major nutrients controls phytoplankton growth and species composition in the tropical North Pacific Ocean. Limnol Oceanogr 38:495–508

Dugdale RC, Wilkerson FP (1998) Silicate regulation of new production in the equatorial Pacific upwelling. Nature 391:270–273

Dugdale RC, Wilkerson FP, Minas JH (1995) The role of a silicate pump in driving new production. Deep-Sea Res 42: 697–719

El-Sayed SZ, Fryxell GA (1993) Phytoplankton antarctic microbiology. In: Friedman EI (ed) Antarctic Microbiology. Wiley-Liss, New York, p 65–122

Falkowski PG (1983) Light-shade adaptation and vertical mixing of marine phytoplankton: a comparative field study. J Mar Res 41:215–237

Falkowski PG (1994) The role of phytoplankton photosynthesis in global biogeochemical cycles. Photosynth Res 39: 235–258

Falkowski PG, Barber RT, Smetacek V (1998) Biogeochemical controls and feedbacks on ocean primary production. Science 281:200–206

Fitzwater SE, Knauer GA, Martin JH (1982) Metal contamination and its effect on primary production measurements. Limnol Oceanogr 27:544–551

Foss P, Guillard RRL, Liaaen-Jensen S (1986) Carotenoids from eucaryotic ultraplankton clones (Prasinophyceae). Phytochemistry 35:119–124

Franck VM, Brzezinski MA, Coale KH, Nelson DM (2000) Iron and silicic acid concentrations regulate Si uptake north and south of the Polar Frontal Zone in the pacific sector of the Southern Ocean. Deep-Sea Res II 47: 3315–3338

Furuya K, Hasumoto H, Nakai T, Nemoto T (1986) Phytoplankton in the Subtropical Convergence during the austral summer: community structure and growth activity. Deep-Sea Res 13:621–630

Gieskes WWC, Kraay GW (1983) Dominance of Cryptophyceae during the phytoplankton spring bloom in the Central North Sea detected by HPLC analysis of pigments. Mar Biol 75:179–185

Glover HE (1985) The physiology and ecology of the marine cyanobacterial genus *Synechococcus.* Adv Aquat Microbiol 3:49–107

Goericke R, Montoya JP (1998) Estimating the contribution of microalgal taxa to chlorophyll *a* in the field—variations of pigment ratios under nutrient- and light-limited growth. Mar Ecol Prog Ser 169:97–112

Goericke R, Repeta DJ (1992) The pigments of *Prochlorococcus marinus*: the presence of divinyl chlorophyll *a* and *b* in a marine procaryote. Limnol Oceanogr 37:425–433

Goericke R, Olson RJ, Shalapyonok A (2000) A novel niche for *Prochlorococcus* sp. in low-light suboxic environments in the Arabian Sea and the Eastern Tropical North Pacific. Deep-Sea Res I 47:1183–1205

Gordon LI, Jennings JC Jr, Ross AA, Krest JM (1993) A suggested protocol for continuous flow automated analysis of seawater nutrients: phosphate, nitrate, nitrite and silicic acid in the WOCE Hydrographic Program and the Joint Global Ocean Flux Study. WHP operations and methods. November 1993. WOCE Hydrographic Program Office, Methods Manual 91-1. Scripps Institution of Oceanography, San Diego, CA

Hansell DA, Feely RA (2000) Atmospheric intertropical convergence impacts surface ocean carbon and nitrogen biogeochemistry in the western tropical Pacific. Geophys Res Lett 27:1013–1016

Higgins HW, Mackey DJ (2000) Algal class abundances, estimated from chlorophyll and carotenoid pigments, in the western Equatorial pacific under El Niño and non-El Niño conditions. Deep-Sea Res I 47:1461–1483

Hoge FE, Wright CW, Swift RN, Yungel JK, Berry RE, Mitchell R (1998) Fluorescence signatures of an iron-enriched phytoplankton community in the eastern equatorial Pacific Ocean. Deep-Sea Res II 45:1073–1082

Hooks CE, Bidigare RR, Keller MD, Guillard RRL (1988) Coccoid eukaryotic marine ultraplankters with four different HPLC pigment signatures. J Phycol 24:571–580

Hutchins DA, Bruland KW (1998) Iron-limited diatom growth and Si:N uptake ratios in a coastal upwelling regime. Nature 393:561–564

Hutchins DA, Witter AE, Butler A, Luther GW III (1999) Competition among marine phytoplankton for different chelated iron species. Nature 400:858–861

Hutchins DA, Sedwick PN, DiTullio GR, Boyd PW, Quéguiner B, Griffiths FB, Crossley AC (2001) Control of phytoplankton growth by iron and silicic acid availability in the subantarctic Southern Ocean: experimental results from the SAZ Project. J Geophys Res 106:31559–31572

Hutchins DA, Hare CE, Weaver RS, Zhang Y and 11 others (2002) Phytoplankton iron limitation in the Humbolt Current and Peru Upwelling. Limnol Oceanogr 47:997–1011

Iriarte JL, Fryxell GA (1995) Micro-phytoplankton at the equatorial Pacific (140° W) during the JGOFS EqPac time series studies: March to April and October 1992. Deep-Sea Res II 42:559–583

Ishizaka J, Harada K, Ishikawa K, Kiyosawa H and 6 others (1997) Size and taxonomic plankton community structure and carbon flow at the equator, 175° E during 1990–1994. Deep-Sea Res II 44:1927–1949

Jacques G (1989) Primary production in the open Antarctic Ocean during the austral summer: a review. Vie Milieu 39: 1–17

Jeffrey SW, Hallegraeff GM (1987) Chlorophyllase distribution in ten classes of phytoplankton: a problem for chlorophyll analysis. Mar Ecol Prog Ser 35:293–304

Jeffrey SW, Wright SW (1994) Photosynthetic pigments in the Haptophyta. In: Leadbeater BSC (ed) The haptophyte algae. Clarendon Press, Oxford, p 111–132

Jeffrey SW, Mantoura RFC, Wright SW (1997) Phytoplankton pigments in oceanography. UNESCO, Paris

Jónasdóttir SH, Kiørboe T, Tang KW, St. John M, Visser AW, Saiz E, Dam HG (1998) Role of diatoms in copepod production: good, harmless or toxic? Mar Ecol Prog Ser 172: 305–308

Kaczmarska I, Fryxell GA (1995) Micro-phytoplankton of the equatorial Pacific: 140° W meridianal transect during the 1992 El Niño. Deep-Sea Res II 42:535–558

Kang SH, Fryxell GA (1991) Most abundant diatom species in water column assemblages from five Leg 119 drill sites in Prydz Bay, Antarctica: distributional patterns. In: Larson B (ed) Proc Ocean Drilling Program, Scientific Results. Texas A&M University Press College Station, TX, p 645–666

Karl DM (1999) A sea of change: biogeochemical variability in the North Pacific Subtropical Gyre. Ecosystems 2:181–214

Karl DM, Letelier RM, Hebel DV, Tupas LM, Dore J, Christian J, Winn CD (1995) Ecosystem changes in the North Pacific subtropical gyre attributed to the 1991–92 El Niño. Nature 373:230–234

Karl DM, Letelier RM, Tupas LM, Dore J, Christian J, Hebel DV (1997) The role of nitrogen fixation in biogeochemical cycling in the subtropical North Pacific Ocean. Nature 388:533–538

Lampert L, Queguiner B, Loyer B, Labasque T, Marie D (2000)

Validity of the phytoplanktonic pigments in determining algal classes on the French Atlantic continental shelf. Seventh International Symposium on Oceanography of the Bay of Biscay, Biarritz, 4–6 April 2000. Institut Francais de Recherche pour l'Exploitation de la Mer, Biarritz, p 113–118

Laws EA, DiTullio GR, Carder KL, Betzer PR, Hawes S (1990) Primary production in the deep blue sea. Deep-Sea Res 37:715–730

Le Borgne R, Rodier R, Le Bouteiller AL, Murray JW (1999) Zonal variability of plankton and particle export flux in the equatorial Pacific upwelling between 165° E and 150° W. Oceanol Acta 22:57–66

Le Bouteiller AL, Blanchot J, Rodier M (1992) Size distribution patterns of phytoplankton in the western Pacific: towards a generalization for the tropical open ocean. Deep-Sea Res II 39:805–823

Legendre LL, Gosselin M (1996) Estimation of N or C uptake rates by phytoplankton using 15N or 13C: revisiting the usual computation formulae. J Plankton Res 19:263–271

Letelier RM, Bidigare RR, Hebel DV, Ondrusek M, Winn CD, Karl DM (1993) Temporal variability of phytoplankton community structure based on pigment analysis. Limnol Oceanogr 38:1420–1437

Lindley ST, Bidigare RR, Barber RT (1995) Phytoplankton photosynthesis parameters along 140° W in the Equatorial Pacific. Deep-Sea Res II 42:441–463

Löscher BM (1999) Relationships among Ni, Cu, Zn, and major nutrients in the Southern Ocean. Mar Chem 67: 67–102

Mackey MD, Mackey DJ, Higgins HW, Wright SW (1996) CHEMTAX—a program for estimating class abundances from chemical markers: application to HPLC measurements of phytoplankton. Mar Ecol Prog Ser 144:265–283

Mackey DJ, Higgins HW, Mackey MD, Wright SW (1997) CHEMTAX user's manual: a program for estimating class abundances from chemical markers—application to HPLC measurements of phytoplankton pigments. CSIRO Marine Laboratory, Hobart

Mackey DJ, Higgins HW, Mackey MD, Holdsworth D (1998) Algal class abundances in the western Equatorial Pacific: estimation from HPLC measurements of chloroplast pigments using CHEMTAX. Deep-Sea Res I 45:1441–1468

Malone TC, Neale PJ (1981) Parameters of light-dependent photosynthesis for phytoplankton size fractions in temperate estuarine and coastal environments. Mar Biol 61: 289–297

Martin JH (1990) Glacial-interglacial CO_2 change: the iron hypothesis. Paleoceanography 5:1–13

Martin JH (1992) Iron as a limiting factor in oceanic productivity. In: Woodhead AD (ed) Primary production and biogeochemical cycles in the sea. Plenum Press, New York, p 123–136

Martin JH, Fitzwater SE, Gordon RM (1990) Iron deficiency limits phytoplankton growth in Antarctic waters. Global Biogeochem Cycles 4:5–12

Mengelt C, Abbott MR, Barth JA, Letelier RM, Measures CI, Vink S (2001) Phytoplankton pigment distribution in relation to silicic acid, iron and the physical structure across the Antarctic Polar Front, 170° W, during austral summer. Deep-Sea Res II 48:4081–4100

Michaels AF, Silver MW (1988) Primary production, sinking fluxes and the microbial food web. Deep-Sea Res 35: 473–490

Minas HJ, Minas M (1992) Net community production in 'high nutrient–low chlorophyll' waters of the tropical and Antarctic Oceans: grazing vs iron hypothesis. Oceanol Acta 15:145–162

Mitchell BG, Holm-Hansen O (1991) Observations and modeling of the Antarctic phytoplankton crop in relation to mixing depth. Deep-Sea Res 38:981–1008

Mitchell GB, Brody E, Holm-Hansen O, McClain CR, Bishop J (1991) Light limitation of phytoplankton biomass and macronutrient utilization in the Southern Ocean. Limnol Oceanogr 36:1662–1677

Moon-van der Staay SY, van der Staay GWM, Guillou L, Vaulot D, Claustre H, Medlin LK (2000) Abundance and diversity of prymnisiophytes in the picoplankton community from the equatorial Pacific Ocean inferred from 18S rDNA sequences. Limnol Oceanogr 45:98–109

Moore JK, Abbott MR, Richman JG (1999) Location and dynamics of the Antarctic Polar Front form satellite sea surface temperature data. J Geophys Res 104:3059–3073

Moore LR, Rocap G, Chisholm SW (1998) Physiology and molecular phylogeny of coexisting *Prochlorococcus* ecotypes. Nature 393:464–467

Mulvenna PF, Savidge G (1992) A modified manual method for the determination of urea in seawater using diacetylmonoxime reagent. Estuar Coast Shelf Sci 34:429–438

Nelson DM, Smith WO Jr (1991) Sverdrup revisited: critical depths, maximum chlorophyll levels and the control of Southern Ocean productivity by the irradiance/mixing regime. Limnol Oceanogr 36:1650–1661

Nelson DM, Tréguer P (1992) Role of silicon as a limiting nutrient to Antarctic diatoms: evidence from kinetic studies in the Ross Sea ice-edge zone. Mar Ecol Prog Ser 80:255–264

Nelson DM, DeMaster DJ, Dunbar RB, Smith WO Jr (1996) Cycling of organic carbon and biogenic silica in the Southern Ocean: estimates of water-column and sedimentary fluxes on the Ross Sea continental shelf. J Geophys Res 101:18519–18532

Nelson DM, Brzezinski MA, Sigmon DE, Franck VM (2001) A seasonal progression of Si limitation in the Pacific sector of the Southern Ocean. Deep-Sea Res II 48:3973–3995

Nodder S, Gall M (1998) Pigment fluxes from the Subtropical Convergence region, east of New Zealand: relationships to planktonic community structure. NZ J Mar Freshw Res 32:441–465

Nolting RF, Gerringa LJA, Swagerman MJW, Timmermans KR, de Baar HJW (1998) Fe (III) speciation in the high nutrient, low chlorophyll Pacific region of the Southern Ocean. Mar Chem 62:335–352

Olson RJ, Chisholm SW, Zettler ER, Armbrust EV (1988) Analysis of *Synechococcus* pigment types in the sea using single and dual beam flow cytometry. Deep-Sea Res 35:425–440

Olson RJ, Chisholm SW, Zettler ER, Altabet MA, Dusenberry JA (1990) Spatial and temporal distributions of prochlorophyte picoplankton in the North Atlantic Ocean. Deep-Sea Res 37:1033–1051

Olson RJ, Sosik HM, Chekalyuk AM, Shalapyonok A (2000) Effects of iron enrichment on phytoplankton in the Southern Ocean during late summer: active fluorescence and flow cytometric analyses. Deep-Sea Res II 47:3181–3200

Orsi AH, Whitworth T III, Nowlin WD Jr (1995) On the meridional extent and fronts of the Antarctic Circumpolar Current. Deep-Sea Res I 42:641–673

Parsons TR, Maita Y, Lalli CM (1984) A manual of chemical and biological methods for seawater analysis. Pergamon Press, New York

Partensky F, Hoepffner N, Li WKW, Ulloa O, Vaulot D (1993) Photoacclimation of *Prochlorococcus* sp. (Prochlorophyta) strains isolated from the North Atlantic and the Mediterranean Sea. Plant Physiol (Rockv) 101:285–296

Peeken I (1997) Photosynthetic pigment fingerprints as indicators of phytoplankton biomass and development in different water masses of the Southern Ocean during austral spring. Deep-Sea Res II 44:261–282

Raimbault P, Slawyk G, Boudjellal B, Coatanoan C and 5 others (1999) Carbon and nitrogen uptake and export in the equatorial Pacific at 150° W: evidence of an efficient regenerated production cycle. J Geophys Res 104:3341–3356

Rubin SI, Takahashi T, Chipman DW, Goddard JG (1998) Primary productivity and nutrient utilization ratios in the Pacific sector of the Southern Ocean based on seasonal changes in seawater chemistry. Deep-Sea Res I 45:1211–1234

Rue EL, Bruland KW (1995) Complexation of iron (III) by natural organic ligands in the Central North Pacific as determined by a new competitive ligand equilibrium/adsorptive cathodic stripping voltammetric technique. Mar Chem 50:117–138

Satoh H, Tanaka H, Koike T (1992) Light condition and photosynthetic characteristics of the subsurface chlorophyll maximum at a station in the Solomon Sea. Jpn J Phycol 40:135–142

Schlüter L, Møhlenberg F, Havskum H, Larson S (2000) The use of phytoplankton pigments for identifying and quantifying phytoplankton groups in coastal areas: testing the influence of light and nutrients on pigment/chlorophyll *a* ratios. Mar Ecol Prog Ser 192:49–63

Sedwick PN, DiTullio GR, Hutchins DA, Boyd P, Griffiths FB, Crossley AC, Trull TW, Quéguiner B (1999) Limitations of algal growth by iron deficiency in the Australian Subantarctic region. Geophys Res Lett 26:2865–2868

Selph KE, Landry MR, Allen CB, Calbet A, Christensen SJ, Bidigare RR (2001) Microbial community composition and growth dynamics in the Antarctic Polar Front and seasonal ice zone during late spring 1997. Deep-Sea Res II 48:4059–4080

Shimada A, Hasegawa T, Umeda I, Nadoya N, Maruyama T (1993) Spatial mesoscale patterns of West Pacific picophytoplankton as analyzed by flow cytometry: their contribution to subsurface chlorophyll maxima. Mar Biol 115:209–215

Smith WO Jr, Anderson RF, Moore JK, Codispoti LA, Morrison JM (2000) The US Southern Ocean joint global ocean flux study: an introduction to AESOPS. Deep-Sea Res II 47:3073–3093

Steinberg DK, Carlson CA, Bates NR, Goldthwait SA, Madin LP, Michaels AF (2000) Zooplankton vertical migration and the active transport of dissolved organic and inorganic carbon in the Sargasso Sea. Deep-Sea Res I 47:137–158

Stoecker DK, Gifford DJ, Putt M (1994) Preservation of marine planktonic ciliates: losses and cell shrinkage during fixation. Mar Ecol Prog Ser 110:293–299

Stolte W, Kraay GW, Noordeloos AAM, Riegman R (2000) Genetic and physiological variation in the pigment composition of *Emiliania huxleyi* (Prymnesiophyceae) and the potential use of its pigment ratios as a quantitative physiological marker. J Phycol 36:529–539

Stramma L, Peterson RG, Tomczak M (1995) The South Pacific Current. J Phys Oceanogr 25:77–91

Sullivan CW, Arrigo KR, McClain CR, Comiso JC, Firestone J (1993) Distribution of phytoplankton blooms in the Southern Ocean. Science 262:1832–1837

Sunda WG, Huntsman SA (1997) Interrelated influence of iron, light and cell size on marine phytoplankton growth. Nature 390:389–392

Suzuki K, Handa N, Kiyosawa H, Ishizaka J (1997) Temporal

and spatial distribution of phytoplankton pigments in the Central Pacific Ocean along 175°E during the boreal summers of 1992 and 1993. J Oceanogr 53:383–396

Takeda S (1998) Influence of iron availability on nutrient consumption ratio of diatoms in oceanic waters. Nature 393: 774–777

Tester PA, Geesey ME, Guo C, Paerl HW, Millie DF (1995) Evaluating phytoplankton dynamics in the Newport River estuary (North Carolina, USA) by HPLC-derived pigment profiles. Mar Ecol Prog Ser 124:237–245

Urban-Rich J, Dagg MJ, Peterson J (2001) Copepod grazing on phytoplankton in the Pacific sector of the Antarctic Polar Front. Deep-Sea Res II 48:4223–4246

van Leeuwe MA, de Baar HJW, Veldhuis MJW (1998a) Pigment distribution in the Pacific region of the Southern Ocean (autumn 1995). Polar Biol 19:348–353

van Leeuwe MA, Timmermans KR, Witte HJ, Kraay GW, Veldhuis MJW, de Baar HJW (1998b) Effects of iron stress on chronic adaptation by natural phytoplankton communities in the Southern Ocean. Mar Ecol Prog Ser 166: 43–52

Vesk M, Jeffrey SW (1987) Ultrastructure and pigments of

two strains of the picoplanktonic alga *Pelagococcus subviridis* (Chrysophyceae). J Phycol 23:322–336

Wilkerson FP, Dugdale RC (1992) Measurements of nitrogen productivity in the Equatorial Pacific. J Geophys Res 97: 669–679

Withers NW, Fiksdahl A, Tuttle RC, Liaaen-Jensen S (1981) Carotenoids of the Chrysophyceae. Comp Biochem Physiol B 68B:345–349

Wright SW, Jeffrey SW (1987) Fucoxanthin pigment markers of marine phytoplankton analysed by HPLC and HPTLC. Mar Ecol Prog Ser 38:259–266

Wright SW, Jeffrey SW, Mantoura RFC, Llewellyn CA, Bjørnland T, Repeta D, Welschmeyer NA (1991) Improved HPLC method for the analysis of chlorophylls and carotenoids from marine phytoplankton. Mar Ecol Prog Ser 77:183–196

Wright SW, Thomas DP, Marchant HJ, Higgins HW, Mackey MD, Mackey DJ (1996) Analysis of phytoplankton of the Australian sector of the Southern Ocean: comparisons of microscopy and size frequency data with interpretations of pigment HPLC data using the 'CHEMTAX' matrix factorisation program. Mar Ecol Prog Ser 144:285–298